This is the peer-reviewed, final accepted version for American Mineralogist, published by the Mineralogical Society of America.
The published version is subject to change. Cite as Authors (Year) Title. American Mineralogist, in press.
DOI: https://doi.org/10.2138/am-2022-8029. http://www.minsocam.org/

Revision 1

A Refined Estimation of Li in Mica by a Machine Learning Method

Lu Wang[1], Cheng Su[1], Luo-Qi Wang[1], J ZhangZhou[1], Qun-Ke Xia[1], and Qin-Yan Wang[1*]

[1]Key Laboratory of Geoscience Big Data and Deep Resource of Zhejiang Province, School of Earth Sciences, Zhejiang University, Hangzhou, 310027, China

Corresponding author: Qinyan Wang (qinyanwang@zju.edu.cn)

ABSTRACT

Li-rich micas are crucial in the exploration for and exploitation of Li resources. The determination of Li in mica using classical bulk chemical methods or in-situ microanalytical techniques is expensive and time-consuming and has a high-quality requirement for micas and reference materials. Although simple linear and nonlinear empirical equations have been proposed, they are inconsistent with the complex physico-chemical mechanisms of Li incorporation and commonly lead to large errors. In this study, we introduce a refined method of multivariate polynomial regression using a machine learning algorithm to estimate Li from multiple major oxide abundances. The performance of our regression model is evaluated using the coefficient of determination (R^2) and the root-mean-square error (RMSE) of the independent test sets. The best-performed models show R^2 of 0.95 and a RMSE of 0.35 wt% for the test set of dataset 1 (all compiled data, n = 2124) and R^2 of 0.96 and a RMSE of 0.22 wt% for the

test set of dataset 2 (only data obtained using in-situ techniques, n = 1386). Our results indicate that integration of electron probe microanalysis and multivariate polynomial regression (based on dataset 1) presents a robust and convenient approach to quantify Li in micas. The application of the proposed approach to micas from central Inner Mongolia, NE China, suggests that in addition to the Weilasituo ore bodies, the Jiabusi granite and greisen and the Shihuiyao metamorphic sediment formation have good potential for Li exploration. Our study also provides preliminary constraints on the genesis of Li deposits.

Keywords: Li in mica, multivariate polynomial regression, machine learning, Li resources

INTRODUCTION

Micas are members of phyllosilicates in which the unit structure consists of one octahedral (O) sheet between two opposing tetrahedral (T) sheets to form a 'TOT' layer. Due to their specific layered structure and flexible crystal lattice, micas are able to accommodate rare elements, such as Li, Rb and Cs, in the interlayer or octahedral structural sites to various extents (Bailey 1984; Rieder et al. 1999).

Lithium is the lightest solid element in the alkali metal group. Due to its unique electrical and mechanical properties, Li is widely used in the ceramic and glass industries, rechargeable batteries, lubricating greases, metallurgy, air treatment, pharmaceuticals, and polymer products (Naumov and Naumova 2010; Bradley et al. 2017). With the increased demand of Li in batteries for electric vehicles (EVs), Li has been recently defined as one of

the strategic metals for green technology (Gruber et al. 2011; Kesler et al. 2012; Linnen et al. 2012; Bradley et al. 2017; Tian et al. 2018). Li-rich micas, such as zinnwaldite and lepidolite, constitute a dominant component of Li resources (Linnen et al. 2012; Bradley et al. 2017; Martin et al. 2017; Rentsch et al. 2018). Quantification of the Li contents in micas is important for the exploitation of Li resources. In addition, a detailed study of composition and microstructure of micas could be used to interpret the complex magmatic-hydrothermal evolution of granitic magmas and associated mineralization (Černý et al. 1985; Henderson et al. 1989; Charoy et al. 1995; Breiter et al. 1997, 2019; Mohamed et al. 1999; Roda et al. 2007; Vieira et al. 2011; Neiva 2013; Breiter et al. 2017a; Garate-Olave et al. 2018; Codeço et al. 2020a).

The electron probe microanalysis (EPMA) is the most frequently used analytical technique to obtain qualitative elemental compositions of solid polished samples at a micrometer scale. However, EPMA cannot be utilized to detect Li because of its low atomic number. Although some classical bulk techniques (such as wet chemistry) and microanalytical methods (such as laser ablation-inductively coupled plasma mass spectrometry (LA-ICP-MS) and secondary ion-mass spectrometry (SIMS)) are capable of determining Li, they are expensive and time-consuming and have high-quality requirements for the analyzed samples and reference materials. Alternatively, an empirical approach has been proposed based on linear or nonlinear correlations between Li_2O and other major components, such as SiO_2, MgO or F, in micas determined by EPMA or other analytical methods (Monier and Robert 1986; Stone et al. 1988; Henderson et al. 1989; Tindle and

Webb 1990; Tischendorf et al. 1997; Tischendorf 1999). Empirical equations, which are either generalized, as those obtained by Tindle and Webb (1990), Tischendorf et al. (1997) and Tischendorf (1999), or formulated for particular cases, are commonly used (Roda-Robles et al. 2006, 2018; Roda et al. 2007; Neiva et al. 2008; Van Lichtervelde et al. 2008; Vieira et al. 2011; Martins et al. 2012; Neiva 2013; Li et al. 2015; Xie et al. 2015; Legros et al. 2016; Ballouard et al. 2020; Yin et al. 2020). Based on 14 published empirical equations, a computer program called LIMICA was developed by Yavuz (2001). However, these empirical equations were proposed for specified types of micas with distinct compositional ranges. Use of these equations for determination of the Li_2O content can be problematic given that some equations are only applicable for a specific Li_2O content. Moreover, the simple correlations between Li_2O and other individual major components are limited to small datasets used in the regression and inconsistent with the complex physico-chemical mechanisms of Li incorporation, which leads to significant errors in their applications (Förster et al. 2005; Thiergärtner 2010; Breiter et al. 2017b; Breiter et al. 2019; Ballouard et al. 2020).

In this study, we use a compilation of >2000 mica compositions from various rock types, including Li_2O and the following 10 major components: SiO_2, Al_2O_3, TiO_2, FeO_T, MgO, MnO, CaO, Na_2O, K_2O, and F. These data are regressed using a multivariate polynomial regression (MPR) based machine learning (ML) method to refine the equation for estimating Li in micas over a wide range of chemical compositions. We then discuss the uncertainties and limitations of the refined equation and compare the performance of the

MPR model with previously published empirical equations. Finally, we apply the refined equation to estimate the Li_2O contents of micas from various types of rocks in central Inner Mongolia, NE China. Our results provide preliminary constraints on the potential for finding new Li resources in NE China.

METHODS

Experimental Datasets

Mica compositions were collected from the published literature using the following criteria: a) Major components of SiO_2, TiO_2, Al_2O_3, FeO_T (total Fe expressed as FeO), MnO, MgO, CaO, Na_2O, K_2O, F, and Li_2O were compiled, whereas H_2O and trace elements were excluded due to the lack of qualified data in most literature sources - otherwise, it is assumed that their influence on the behavior of Li is minor and can be ignored; b) The compiled oxides were determined using either in-situ microanalysis, such as EPMA, LA-ICP-MS or SIMS, or classical bulk chemistry on pure mica separates; c) Li contents were obtained from the grains or spots that were the same as or close to those from which the other oxides were analyzed; and d) The micas that occurred as post-formation residuals modified at disequilibrium conditions or showed abnormal compositions were excluded. To avoid computational errors, the compositions that are below detection limits were set to 0.000001 wt%, and the data with symbols "<" and "<<" were recalculated by multiplying them with 0.8 and 0.2, respectively. After this data cleaning, a total of 2124

compositions from 94 published literature sources (years 1960–2020) were used for further data processing.

Considering the varying accuracies in the mica compositions, two types of datasets were used for regression: dataset 1 consisting of the whole compiled data (n = 2124), and dataset 2 screened to contain data determined by two or more in-situ techniques on the same or closely located spots (n = 1386) (Table S1). In dataset 1, most of the micas are from granites, pegmatites and other granitic rocks, and the rest are from greisens, carbonatites, kimberlites, lamproites, lherzolites and metamorphic rocks including eclogites, migmatites, gneisses and schists. They cover a wide range of compositions with 31.40–59.65 wt% SiO_2, 0–8.56 wt% TiO_2, 0.04–38.77 wt% Al_2O_3, 0–35.84 wt% FeO_T, 0–7.60 wt% MnO, 0–29.98 wt% MgO, 0–3.42 wt% CaO, 0–2.24 wt% Na_2O, 4.79–12.57 wt% K_2O, 0–10.34 wt% F, and 0–7.70 wt% Li_2O. In the classification diagram of Tischendorf et al. (1997), these micas plot in a broad field covering (Li-) phengite, (Li-)muscovite, zinnwaldite, lepidolite, protolithionite, siderophyllite, lepidomelane, Fe-biotite, Mg-biotite and phlogopite, with a minor portion of them plotting in the taeniolite and alumino-phlogopite fields (Fig. 1a). Compared to dataset 1, dataset 2 contains similar rock types but their compositional range is narrower: 33.50–59.17 wt% SiO_2, 0.04–37.88 wt% Al_2O_3, 0–27.32 wt% FeO_T , 0–3.86 wt% MnO, 0–1.38 wt% Na_2O, 5.62–11.62 wt% K_2O, and 0–6.93 wt% Li_2O. As shown in the classification diagram, dataset 2 is concentrated in the (Li-) phengite, (Li-)muscovite and phlogopite fields, with fewer compositions in the fields of other mica types (Fig. 1b). Lepidomelane, taeniolite

126 and alumino-phlogopite compositions are absent in dataset 2.

127

128 **Regression analysis**

129 Regression analysis is one of the classical models that are commonly used in the ML
130 algorithms. It is a statistical method for estimating the relationship between a dependent
131 variable *y* and one or more independent variables *x*. The linear regression model is the
132 most common and basic statistical method, the equation of which can be expressed as:

133 $$y = \beta_0 + \sum_{i=1}^{k} \beta_i x_i + \varepsilon \quad (1)$$

134 where β_0 is the intercept, β_i is the linear effect parameter, and ε represents the error. In
135 particular, the linear relationship between one dependent variable and one independent
136 variable is called simple linear regression. But in most cases, especially those related to
137 complex geological processes, the observational data cannot be well modeled by a simple
138 linear regression model. Instead, multivariate polynomial regression (MPR) is considered
139 to be more appropriate to model nonlinear relationships between variables (Draper and
140 Smith 1998). Taking bivariate quadratic polynomial regression as an example, the model
141 is formulated as:

142 $$y = \beta_0 + \beta_1 x_1 + \beta_2 x_2 + \beta_{11} x_1^2 + \beta_{22} x_2^2 + \beta_{12} x_1 x_2 + \varepsilon \quad (2)$$

143 where β_0 is the intercept, β_1 and β_2 are the linear effect parameters, β_{11} and β_{22} are the
144 quadratic effect parameters, β_{12} is the interaction effect parameter, and ε is the error.
145 This equation can be expressed in a matrix form as:

146 $$\boldsymbol{Y} = \boldsymbol{\beta X} + \boldsymbol{\varepsilon} \quad (3)$$

This is the peer-reviewed, final accepted version for American Mineralogist, published by the Mineralogical Society of America.
The published version is subject to change. Cite as Authors (Year) Title. American Mineralogist, in press.
DOI: https://doi.org/10.2138/am-2022-8029. http://www.minsocam.org/

where $\boldsymbol{Y}$ is a vector of dependent variables, $\boldsymbol{X}$ represents a designed vector of independent variables including a constant term of 1, x_1, x_2, x_1^2, x_1x_2 and x_2^2, $\boldsymbol{\beta}$ is a vector of parameters denoted by β_0, β_1, β_2, β_{11}, β_{12}, and β_{22} and $\boldsymbol{\varepsilon}$ refers to a vector of random errors. Assuming m training items, the model can be written as a system of linear equations:

$$\begin{bmatrix} y^1 \\ y^2 \\ \vdots \\ y^m \end{bmatrix} = \begin{bmatrix} \beta_0 \\ \beta_1 \\ \beta_2 \\ \beta_{11} \\ \beta_{12} \\ \beta_{22} \end{bmatrix} \times \begin{bmatrix} 1 & x_1^1 & x_2^1 & (x_1^1)^2 & x_1^1x_2^1 & (x_2^1)^2 \\ 1 & x_1^2 & x_2^2 & (x_1^2)^2 & x_1^2x_2^2 & (x_2^2)^2 \\ \vdots & \vdots & \vdots & \vdots & \vdots & \vdots \\ 1 & x_1^m & x_2^m & (x_1^m)^2 & x_1^mx_2^m & (x_2^m)^2 \end{bmatrix} + \begin{bmatrix} \varepsilon^1 \\ \varepsilon^2 \\ \vdots \\ \varepsilon^m \end{bmatrix} \quad (4)$$

Similarly, the general form of multivariate polynomial regression (degree of i) is:

$$\begin{bmatrix} y^1 \\ y^2 \\ \vdots \\ y^m \end{bmatrix} = \begin{bmatrix} 1 & x_1^1 & \dots & x_n^1 & (x_1^1)^2 & x_1^1x_2^1 & \dots & (x_n^1)^2 & (x_1^1)^3 & (x_1^1)^2x_2^1 & \dots & x_{n-1}^1(x_n^1)^{i-1} & (x_n^1)^i \\ 1 & x_1^2 & \dots & x_n^2 & (x_1^2)^2 & x_1^2x_2^2 & \dots & (x_n^2)^2 & (x_1^2)^3 & (x_1^2)^2x_2^2 & \dots & x_{n-1}^2(x_n^2)^{i-1} & (x_n^2)^i \\ \vdots & \vdots & \vdots & \vdots & \vdots & \vdots & \vdots & \vdots & \vdots & \vdots & \vdots & \vdots & \vdots \\ 1 & x_1^m & \dots & x_n^m & (x_1^m)^2 & x_1^mx_2^m & \dots & (x_n^m)^2 & (x_1^m)^3 & (x_1^m)^2x_2^m & \dots & x_{n-1}^m(x_n^m)^{i-1} & (x_n^m)^i \end{bmatrix}$$

$$\times \begin{bmatrix} \beta_0 \\ \beta_1 \\ \vdots \\ \beta_n \\ \beta_{11} \\ \beta_{12} \\ \vdots \\ \beta_{nn} \\ \beta_{111} \\ \beta_{112} \\ \vdots \\ \beta_{(n-1)\underbrace{n..n}_{i-1}} \\ \beta_{\underbrace{n..n}_{i}} \end{bmatrix} + \begin{bmatrix} \varepsilon^1 \\ \varepsilon^2 \\ \vdots \\ \varepsilon^m \end{bmatrix} \quad (5)$$

This is the peer-reviewed, final accepted version for American Mineralogist, published by the Mineralogical Society of America.
The published version is subject to change. Cite as Authors (Year) Title. American Mineralogist, in press.
DOI: https://doi.org/10.2138/am-2022-8029. http://www.minsocam.org/

155 The parameter $\boldsymbol{\beta}$ is generally estimated using the ordinary least square (OLS) method by
156 minimizing the sum of squared residuals (SSR), where

157 $$\mathrm{SSR} = \left(\boldsymbol{\beta X}-\boldsymbol{Y}\right)^{\mathrm{T}}\left(\boldsymbol{\beta X}-\boldsymbol{Y}\right) \quad (6)$$

158 Theoretically, a sufficiently high-degree polynomial can approximate any nonlinear
159 relationships (Draper and Smith 1998). Thus, it is reasonable and appropriate to use the
160 MPR to express the complicated relationship between Li_2O and other major components
161 in mica. We applied a MPR-based ML algorithm with Python coding in the open-source
162 Anaconda distribution. The code is available on GitHub at the following URL
163 (https://github.com/luwang9103/MPR-Li-mica.git). The degree of an approximate
164 polynomial was chosen by testing the performance of model fitting at each step with a
165 successively increasing degree, keeping it as low as possible. Given the problems of
166 multicollinearity and overfitting, which commonly occur in the MPR, a method of elastic
167 net regularization was performed (Zou and Hastie 2005). Elastic net is a regularized
168 regression method that linearly combines the L1 and L2 penalties of the lasso and ridge
169 methods and aims at minimizing the loss function of

170 $$J(\boldsymbol{\beta}) = \frac{1}{2}\left(\boldsymbol{\beta X}-\boldsymbol{Y}\right)^{\mathrm{T}}\left(\boldsymbol{\beta X}-\boldsymbol{Y}\right)+\alpha\rho\|\boldsymbol{\beta}\|_1+\frac{\alpha(1-\rho)}{2}\|\boldsymbol{\beta}\|_2^2 \quad (7)$$

171 where ρ is the mixing parameter between lasso (ρ=0) and ridge (ρ=1) and α is a
172 constant coefficient. This method deals with bias-variance tradeoff to avoid overfitting
173 and reduces the influence of multicollinearity simultaneously. Multicollinearity leads to
174 small eigenvalues of $\boldsymbol{X}^{\mathrm{T}}\boldsymbol{X}$, thus the variance of the regression coefficient $\boldsymbol{\beta}$ can be very
175 large with the OLS method (equation 6). The regularization constructs an alternative

This is the peer-reviewed, final accepted version for American Mineralogist, published by the Mineralogical Society of America.
The published version is subject to change. Cite as Authors (Year) Title. American Mineralogist, in press.
DOI: https://doi.org/10.2138/am-2022-8029. http://www.minsocam.org/

176 estimator by adding penalties that gives a smaller variance of **β**. Specifically, the ridge
177 shrinks the coefficients of less important variables to near zero, and the lasso reduces the
178 number of irrelevant variables. The elastic net method combines the advantages of the two
179 regressions (Zou and Hastie 2005). Because two parameters of ρ and α are needed in
180 the elastic net, we performed a two-dimension grid search to tune the parameters by using
181 nested loops. We iterated through the values from 0.1 to 1 for both parameters with a step
182 size of 0.1. After 100 iterations, the optimal parameter pair that gives the highest R^2
183 scores was chosen.
184 The two datasets of this work were treated individually when performing the ML. For
185 both datasets, 70% of the data were used as a training set to yield the regression model
186 and 30% were used as a test set to evaluate the accuracy and uncertainty of the model.
187 The split of the datasets was based on a random sampling method. We conducted 20
188 replications of the random splitting, training and testing procedures to provide a robust
189 estimation of the predictive performance, which is evaluated with the coefficient of
190 determination (R^2) and the root-mean-square error (RMSE).
191

192 **RESULTS**

193 Our results show that a cubic polynomial with regularized parameters of $\rho = 0.1$ and
194 $\alpha = 0.1$ exhibits a good performance of regression. For the dataset 1 model, the R^2 values
195 calculated from the training set are stable at 0.93–0.96 with RMSE values of 0.30–0.38
196 wt%, while the R^2 values calculated from the test set vary from 0.87 to 0.95 with RMSE

values of 0.35–0.54 wt% (Table 1). The results of the best predictive performance are visualized in figure 2. Both the training and test sets display good correlations between the predicted and measured Li_2O values, although minor deviations from the one to one straight line exist (Fig. 2a). In the error distribution diagram, 84% predictions in the test set have errors less than the RMSE (0.35 wt%) and only 3% predictions display deviations higher than 1 wt% (Fig. 3a). Comparatively, the dataset 2 model performs better with R^2 values of 0.96–0.97 and RMSE values of 0.19–0.22 wt% for the training set and R^2 values of 0.92–0.96 and RMSE values of 0.22–0.33 wt% for the test set (Table 1). In the predicted Li_2O vs. measured Li_2O diagram, the best-performed training and test sets exhibit remarkable positive trends and most of the predicted values plot close to the 1:1 straight line (Fig. 2b). Except for one data with the error of 1.14 wt%, the predicted values of the test set show deviations within 1 wt%, 80% of which are less than the RMSE of 0.22 wt% (Fig. 3b).

DISCUSSIONS

Accuracy and uncertainty of the MPR method

The high R^2 (>0.87) and low RMSE (<0.54 wt%) values for the test sets, which were not used during the training procedure, characterize the robust and accurate prediction level of the MPR method. However, the fitting and predictive performance of the dataset 2 model is better than that of the dataset 1 model. Regression analysis is strongly influenced by the quality of the original data. The mica compositions of dataset 2 are limited to those

obtained by the combined EPMA and SIMS/LA-ICP-MS methods on the same or closely associated spots representing homogeneous or nearly homogeneous compositions of the analyzed micro-domains. The analytical errors are less than ±2% for most major elements and less than ±3–10% for Li_2O with various abundances (Kalt et al. 2001; Roda-Robles et al. 2012; Forni et al. 2016; Xie et al. 2018). In addition to in-situ microanalyses, dataset 1 contains bulk chemical analyses by classical wet chemistry, atomic spectrometry and X-ray fluorescence analysis, which display similar analytical errors with in-situ techniques (Barrière and Cotten 1979; Neiva 1980; Silva and Neiva 1990; Gomes and Neiva 2005). However, these bulk chemical analyses may cause serious biases when the mica separates contain inclusions of other minerals or show zoned or heterogeneous compositions, which is commonly the case in rare metal occurrences related to magmatic differentiation and hydrothermal processes (Charoy and Noronha 1996). Propagation of these inherited measurement errors leads to the relatively larger uncertainties in the dataset 1 model.

Other factors that affect the uncertainties of both dataset models may include: 1) The total Fe content is used for regression since ferric and ferrous iron cannot be distinguished in most studies; 2) Some trace elements that may be enriched in particular micas and have strong correlations with lithium, such as Rb_2O, Cs_2O, SnO_2 and Ga_2O_3 (Tischendorf et al. 2001), have not been compiled; and 3) Both in-situ and bulk analyses of micas show large analytical errors in low concentration ranges.

This is the peer-reviewed, final accepted version for American Mineralogist, published by the Mineralogical Society of America.
The published version is subject to change. Cite as Authors (Year) Title. American Mineralogist, in press.
DOI: https://doi.org/10.2138/am-2022-8029. http://www.minsocam.org/

Comparison with previous methods

The empirical approach of calculating Li_2O in micas on the basis of major component correlations has been employed for a long time. Based on a dataset of approximately 400 wet chemical analyses, Tindle and Webb (1990) gave an empirical equation of $Li_2O = 0.287 \times SiO_2 - 9.552$ for Li-bearing trioctahedral micas with MgO <8 wt%. Tischendorf et al. (1997) proposed a revised equation of $Li_2O = 0.289 \times SiO_2 - 9.658$ (n = 232), which was applicable to trioctahedral micas with Li_2O >0.6 wt%, MgO <3 wt% and SiO_2 >34 wt% (Tischendorf 1999). The other good non-linear equations (R^2 >0.8) relating Li_2O and individual major components, such as MgO and F, for trioctahedral and dioctahedral micas are summarized in Table 2.

For comparison, we use the same test sets of the best-performed dataset 1 and dataset 2 models to calculate Li_2O contents by applying these empirical equations. When using the test set of the dataset 1 model (total n = 638), <170 micas match the recommended ranges of validity for the SiO_2 and Li_2O relations (Table 3). As illustrated in Figs. 4a and 4b, the calculated Li_2O contents (orange cross) are more scattered than those predicted by the MPR, with R^2 of 0.82 and a RMSE of 0.73 wt% for the equation of Tindle and Webb (1990) and R^2 of 0.68 and a RMSE of 0.88 wt% for the equation of Tischendorf et al. (1997). The nonlinear Li_2O-MgO correlation of Tischendorf et al. (1997) is applicable to a larger number of micas (n = 220), but the predicted results show serious deviations from the measured values (Fig. 4c). The two Li_2O-F equations for the trioctahedral micas (n >300) perform well, though the predicted results are biased to higher values in the

260 Li_2O range of 3–5 wt% with overestimations reaching 5 wt% (Figs. 4d-e). Their overall
261 R^2 and RMSE values are 0.78–0.82 and 0.85–0.95 wt%, respectively (Table 3). The
262 Li_2O-F equation for the dioctahedral micas (n = 306) is limited to Li_2O contents of less
263 than 3 wt% and the calculated results are worse than the MPR predictions with R^2 of 0.51
264 and a RMSE of 0.40 wt% (Fig. 4f; Table 3). Each of the four renewed Li_2O-MgO
265 equations of Tischendorf (1999) is for a distinct mica type. However, because these
266 mica-types are not quantitatively defined, we are unable to apply these equations to our
267 data, and hence they are not further discussed here. To reduce the influences of analytical
268 errors, we further compare the predictive performances among different methods using
269 the test set of the dataset 2 model. The results from empirical equations are similar to
270 those obtained from dataset 1 with relatively higher accuracy but are still worse than
271 those of the MPR method (Fig. 5; Table 3).
272 Above all, our study indicates that although the previously proposed equations show a
273 good fit for the dataset used in original regression, their application to independent micas
274 are burdened with errors to different extents. Moreover, these equations are only
275 available for either trioctahedral or diotahedral micas with specific compositional ranges.
276 It is sometimes contradictory that the Li_2O content can be used as an application criterion
277 where Li_2O is absent for the mica to be calculated (Table 2). As shown in figures 4 and 5,
278 the predicted data falling outside the validity range of empirical equations (blue cross)
279 could lead to large errors. In contrast, our MPR method has a better generalization

This is the peer-reviewed, final accepted version for American Mineralogist, published by the Mineralogical Society of America.
The published version is subject to change. Cite as Authors (Year) Title. American Mineralogist, in press.
DOI: https://doi.org/10.2138/am-2022-8029. http://www.minsocam.org/

capability that is applicable to different types of micas with a wider range of compositions, thus exhibiting a more precise and accurate predictive performance.

On the other hand, some authors use good linear correlations (R^2 >0.9) between F and Li_2O that were obtained from a limited amount of analytical data (in-situ techniques) to estimate the Li_2O contents of other unmeasured micas (Table 2; Roda et al. 2007; Van Lichtervelde et al. 2008; Vieria et al. 2011; Codeço et al. 2020a). The positive relationship between F and Li_2O is consistent with the incompatible behavior of these two elements, especially during magmatic or hydrothermal processes. However, in the F vs. Li_2O diagrams (Fig. 6), both dioctahedral and trioctahedral micas from dataset 2 show overall scattered linear trends (R^2 of 0.52 and 0.79). The influence of analytical error can be neglected due to the high precision of dataset 2. Thus, it is considered that only few micas with particular occurrences and compositions may yield strong linear correlations between Li_2O and F and the equations based on their relations have a limited application.

IMPLICATIONS

Implications for estimating Li in micas

The simplified formula of micas is given as $IM_{2\text{-}3}\square_{1\text{-}0}T_4O_{10}A_2$, where *I* represents interlayer cations commonly composed of K, Na, Ca, Ba and rarely Rb, Cs, and NH_4; *M* refers to either trioctahedral or dioctahedral cations of Li, Fe^{2+}, Fe^{3+}, Mg, Al, Ti, Mn^{2+}, Mn^{3+}, Zn, Cr, and V; □ represents a vacancy; *T* refers to tetrahedral cations generally including Si, Al, Fe^{3+} and rarely B and Be; and *A* refers to anions of F, OH, Cl, and S

(Rieder et al. 1999). Lithium enters the mica crystal lattice via several competing substitution mechanisms, which include $3Li^{VI} \leftrightarrow Al^{VI} + 2\square^{VI}$, $Si^{IV} + 2Li^{VI} \leftrightarrow 2Al^{VI} + \square^{VI}$, and $2Si^{IV} + Li^{VI} \leftrightarrow 3Al^{Tot}$ for Al-rich micas, and $Si^{IV} + Li^{VI} \leftrightarrow Al^{IV} + R^{VI}$, $Si^{IV} + 2Li^{VI} \leftrightarrow 3R^{VI}$ and $Al^{VI} + Li^{VI} \leftrightarrow 2R^{VI}$, where R^{VI} = Fe+Mg+Mn, for Fe-rich micas (Foster 1960; Henderson et al. 1989; Charoy et al. 1995; Roda-Robles et al. 2006; Roda et al. 2007; Vieira et al. 2011; Martins et al. 2012; Breiter et al. 2017b). The incorporation of F in the OH site has a close correlation with the incorporation of Li in the octahedral site (Foster 1960; Roda et al. 2007; Van Lichtervelde et al. 2008). In addition, the substitutions in the octahedral and tetrahedral sites influence the size of the interlayer site, which is further associated with the various occupations of interlayer cations (Van Lichtervelde et al. 2008). Therefore, the incorporation of Li in micas is controlled by complex physico-chemical mechanisms. The previous empirical equations that were derived from the correlations between Li_2O and individual major components, such as SiO_2, MgO and F, using a limited dataset led to the loss of information, which is interpreted as the main reason for their biased estimations.

The MPR method proposed in this study is based on a statistical evaluation of large datasets that contain 10 major components (SiO_2, Al_2O_3, MgO, FeO_T, MnO, TiO_2, CaO, Na_2O, K_2O, F) and Li_2O. Although the variables used for regression cannot cover all the factors that affect the Li incorporation, the MPR shows a more precise, accurate and robust prediction power than the empirical equations. Moreover, it is generalized to almost all types of micas and the input oxides can be easily obtained by EPMA. It is

This is the peer-reviewed, final accepted version for American Mineralogist, published by the Mineralogical Society of America.
The published version is subject to change. Cite as Authors (Year) Title. American Mineralogist, in press.
DOI: https://doi.org/10.2138/am-2022-8029. http://www.minsocam.org/

noted that although the dataset 1 model yields relatively larger uncertainties than the dataset 2 model, the former is still recommended here because it covers a wider range of mica types and compositions. Considering the limited number of alumino-phlogopite and tainiolite in the compilation, our method may cause large errors for these two mica types. The micas that have undergone modification under disequilibrium conditions are not suggested for prediction. In this study, a user-friendly Excel spreadsheet is provided for calculating Li_2O from EPMA data (Table S2).

Application of the MPR to exploration of Li deposits in NE China

Recent studies have discovered a series of Li-W-Sn-Nb-Ta deposits in central Inner Mongolia of northeastern China, which are located at depth in a previously explored Weilasituo ore district dominated by volcanic-subvolcanic Cu-Pb-Zn-Ag deposits (Fig. 7; Wang et al. 2017; Li et al. 2018; Gao et al. 2019). More than 600 Kt of ore with an average Li grade of 1.25 wt% have been estimated in this region, indicative of good prospects for exploitation (Li et al. 2017). Gao et al. (2019) conducted a detailed analysis of mica compositions from the Weilasituo ore bodies. Their results reflect the predominant ore minerals of zinnwaldites, which contain 3.5–5 wt% Li_2O contents measured by LA-ICP-MS (Gao et al. 2019). To test the predictive capability of our method in the specific case, we start by applying the Excel spreadsheet provided in this study to predict the Li_2O contents of the Weilasituo micas (60 analyses) from Gao et al. (2019), which have not been used in the ML. The predicted values are in good agreement

This is the peer-reviewed, final accepted version for American Mineralogist, published by the Mineralogical Society of America.
The published version is subject to change. Cite as Authors (Year) Title. American Mineralogist, in press.
DOI: https://doi.org/10.2138/am-2022-8029. http://www.minsocam.org/

343 with the measured Li_2O contents within limited errors of ± 0.5 wt% (Fig. 8a). The
344 prediction of the Li_2O-SiO_2 equations is comparable with our method (Figs. 8b-c), but the
345 Li_2O-MgO and Li_2O-F equations perform worse (Figs. 8d-f).
346 To further explore the potential Li resources in central Inner Mongolia of NE China, we
347 collected 12 rock samples on the basis of geochemical anomalies, including granites,
348 greisens, pegmatites, quartz porphyry and metamorphic rocks from the Weilasituo, Jabusi,
349 Shihuiyao and Bayangen areas (Fig. 7). Micas in these samples occur as subhehral to
350 euhedral crystals and represent the main Li-bearing minerals. Representative
351 compositional profiles of 2 to 6 mica grains were performed by EPMA for each sample.
352 The analyzed method and chemical compositions of micas (471 analyses) are given in
353 Test S1 and Table S3. We predict 2.66–4.43 wt% Li_2O for micas from the Weilasituo
354 quartz porphyry (sample WLST-5), which is comparable with the reported values of 3.72–
355 4.22 wt% Li_2O (Gao et al. 2019), while micas from a plagioclase gneiss (sample WLST-1)
356 of the metamorphic basement mainly consists of Mg-biotites with predicted Li_2O contents
357 of 0–0.24 wt% (Fig. 9). In addition to the Weilasituo mining area, the Jiabusi area seems
358 to have a good potential for Li resources in terms of dominant Li-rich micas in the granite
359 and greisen samples (samples JBS-1-4), with the compositions ranging from Li-phengite
360 and zinnwaldite to lepidolite (Fig. 9). Especially, lepidolites in sample JBS-2 show Li_2O
361 contents of 4.80–6.69 wt%, which are higher than the zinnwaldites in the Weilasituo ore
362 bodies (up to 4.85 wt% Li_2O; Gao et al. 2019). In the Bayangen area, micas from the
363 granite, pegmatite and quartz schist (samples BYG-6-8) are phengites with low Li_2O

abundances of 0–0.44 wt% (Fig. 9). In the Shihuiyao area, the greisen (sample SHY-1) and granite (sample SHY-3) contain phengite-muscovite with 0–0.72 wt% Li_2O, while the surrounding metamorphic sedimentary rock (sample SHY-2) contains Li-bearing phengite with higher Li_2O of 0.60–2.93 wt% (mostly >2 wt%; Fig. 9). In summary, our work suggests that Li in micas from the Jiabusi granite and greisen (avg. Li_2O 3.35 wt%) and the Shihuiyao metamorphic sediment (avg. Li_2O 2.44 wt%) reach industrial standards and have good prospects for exploitation.

Furthermore, the various types and compositions of micas in rocks from different occurrences may provide crucial mineralogical constraints on metallogenic processes. In the Weilasituo area, the Li_2O contents of Mg-biotites from the plagioclase gneiss of the metamorphic basement (0–0.24 wt% Li_2O) are lower than those of zinnwaldites from the plagioclase gneiss surrounding the ore veins (4.28–4.49 wt% Li_2O; Gao et al. 2019), indicating that the wall rock was probably metasomatized by ore-bearing hydrothermal fluids. In the Shihuiyao area, micas from the metamorphic sediment are enriched in Li_2O relative to the intrusive granite or greisen, which probably indicates an input of Li from Li-rich sources during sedimentation. Metamorphism may also contribute the increase of Li in micas.

Considering that Li preferentially partitions into the melt during partial melting or fractionation processes, the variations of Li at the mineral scale is routinely used as a geochemical tracer for understanding and reconstruction of magmatic and mineralizing processes (Charoy et al. 1995; Henderson et al. 1989; Neiva 2013; Breiter et al. 2017a;

385 Garate-Olave et al. 2018; Bretier et al. 2019). Back-scattered electron (BSE) images show
386 that most mica grains in the studied samples display heterogeneous or zoned patterns.
387 The chemical profiles determined by EPMA with Li_2O calculated by the MPR method
388 exhibit similar compositional characteristics, especially for the Jiabusi samples, which
389 display various compositions for individual grains (Table S3). As illustrated in figure 10a,
390 a mica grain from sample JBS-1 has core-to-rim zoning, characterized by a wide, darker
391 core of zinnwaldite (Li <2.2 apfu) and a thin, lighter rim of lepidolite (Li >2.2 apfu), with
392 their contact being regular. The lepidolite crystals from sample JBS-2 show a similar
393 compositional zoning with a BSE-dark core and a BSE-light rim (Fig. 10b). A
394 quantitative analysis demonstrates that Li enrichment in the rim domain (Li >3 apfu)
395 exceeds that of the core domain (Li <3 apfu) (Fig. 10b). The core-rim patterns and
396 various chemical compositions of micas in the Jiabusi area probably indicate that the Li
397 mineralization is related to highly fractionated granitic magmas, although more work is
398 needed to confirm this in the future. It is noted that the application of in-situ techniques to
399 obtain complex compositional features in mica grains is sometimes hampered by the large
400 beam diameter (30–100 μm for LA-ICP-MS) required for analysis. Integration of EPMA
401 (beam diameter ≤5 μm) and MPR methods presents a robust and convenient approach for
402 conducting microanalysis of Li in micas.
403

404 **CONCLUSIONS**

Our study provides a new MPR analysis using a ML algorithm to estimate the Li_2O contents of mica from their compositions obtained by EPMA. This method is more precise, accurate and generalized than the previously published empirical equations. Application of MPR to samples from central Inner Mongolia, NE China, suggests that in addition to the Weilasituo ore bodies, Li-rich micas from the Jiabusi granite and greisen and the Shihuiyao metamorphic sediment formation have good prospects for Li exploitation. Integration of EPMA and MPR provides a robust and convenient approach for conducting microanalysis of Li in micas. Detailed analysis of mica compositions in different rocks enhances our understanding of the mineralization in the Jiabusi and Shihuiyao ore bodies, with the former likely being associated with Li-enriched sedimentary sources and the latter likely relating to highly fractionated granitic magmas.

ACKNOWLEDGEMENTS

This study was supported by the Inner Mongolia Autonomous Region Geological Exploration Fund Project (No. 2017-YS02), the National Natural Science Foundation of China (No. 41830212), and the Fundamental Research Funds for the Central Universities. The collection of rock samples in central Inner Mongolia was supported and assisted by Wencai Yang and Meixia Su. We thank Xiaohong Huang, Rui Shi, Danfeng Qi, Zeqing Wang, Yang Wang, Sijie Wang, Yuyang Hou, Jintao Zhou, Can He, Yifan Xu, Xiaodong Wu, Naixiao Xu, Xinru Li, Wenjun Zhou, Linfeng Liao, Xi Lu, Luyao Jin, Shuang Liu, Kaiteng Huang, Sihui Chen, Lingchang Kong, Yiheng Zhang, and Boqin Xiong for their

help in the ML. We thank Eero Hanski and Stephen T. Johnston for polishing the English.

REFERENCES

Bailey, S.W., Ed. (1984) Reviews in Mineralogy, Vol. 13—Micas, 584 p. Mineralogical Society of America, Washington, DC.

Ballouard, C., Elburg, M.A., Tappe, S., Reinke, C., Ueckermann, H., and Doggart, S. (2020) Magmatic-hydrothermal evolution of rare metal pegmatites from the Mesoproterozoic Orange River pegmatite belt (Namaqualand, South Africa). Ore Geology Reviews, 116, 103252.

Barrière, M., and Cotten, J. (1979) Biotites and associated minerals as markers of magmatic fractionation and deuteric equilibration in granites. Contributions to Mineralogy and Petrology, 70, 183–192.

Bradley, D.C., Stillings, L.L., Jaskula, B.W., Munk, LeeAnn, and McCauley, A.D. (2017) Lithium, chap. K of Schulz, K.J., DeYoung, J.H., Jr., Seal, R.R., II, and Bradley, D.C., eds., Critical mineral resources of the United States—Economic and environmental geology and prospects for future supply. U.S. Geological Survey Professional Paper, 1802, K1–K21.

Breiter, K., Frýda, J., Seltmann, R., and Thomas, R. (1997) Mineralogical evidence for two magmatic stages in the evolution of an extremely fractionated P-rich rare-metal granite: The Podlesí stock, Krušné Hory, Czech Republic. Journal of Petrology, 38, 1723–1739.

447 Breiter, K., Ďurišová, J., Hrstka, T., Korbelová, Z., Hložková Vaňková, M., Vašinová
448 Galiová, M., Kanický, V., Rambousek, P., Knésl, I., Dobeš, P., and others (2017a)
449 Assessment of magmatic vs. metasomatic processes in rare-metal granites: A case
450 study of the Cínovec/Zinnwald Sn–W–Li deposit, Central Europe. Lithos, 292–293,
451 198–217.
452 Breiter, K., Vaňková, M., Galiová, M.V., Korbelová, Z., and Kanický, V. (2017b) Lithium
453 and trace-element concentrations in trioctahedral micas from granites of different
454 geochemical types measured via laser ablation ICP-MS. Mineralogical Magazine, 81,
455 15–33.
456 Breiter, K., Hložková, M., Korbelová, Z., and Galiová, M.V. (2019) Diversity of lithium
457 mica compositions in mineralized granite–greisen system: Cínovec Li-Sn-W deposit,
458 Erzgebirge. Ore Geology Reviews, 106, 12–27.
459 Černý, P., Meintzer, R.E., and Anderson, A.J. (1985) Extreme fractionation in
460 rare-element granitic pegmatites: selected examples of data and mechanisms.
461 Canadian Mineralogist, 23, 381–421.
462 Charoy, B., and Noronha, F. (1996) Multistage growth of a rare-element, volatile-rich
463 microgranite at argemela (Portugal). Journal of Petrology, 37, 73–94.
464 Charoy, B., Chaussidon, M., and Noronha, F. (1995) Lithium zonation in white micas
465 from the Argemela microgranite (central Portugal): an in-situ ion-,
466 electron-microprobe and spectroscopic investigation. European Journal of
467 Mineralogy, 7, 335–352.

468 Codeço, M.S., Weis, P., Trumbull, R.B., Van Hinsberg, V., Pinto, F., Lecumberri-Sanchez,
469 P., and Schleicher, A.M. (2020a) The imprint of hydrothermal fluids on
470 trace-element contents in white mica and tourmaline from the Panasqueira W–Sn–
471 Cu deposit, Portugal. Mineralium Deposita.
472 https://doi.org/10.1007/s00126-020-00984-8.
473 Draper, N.P., and Smith, H. (1998) Applied Regression Analysis, Third Edition. John
474 Wiley and Sons, Inc, 736 p.
475 Forni, F., Bachmann, O., Mollo, S., De Astis, G., Gelman, S.E., and Ellis, B.S. (2016)
476 The origin of a zoned ignimbrite: Insights into the Campanian Ignimbrite magma
477 chamber (Campi Flegrei, Italy). Earth and Planetary Science Letters, 449, 259–271.
478 Förster, H.J., Tischendorf, G., Rhede, D., Naumann, R., Gottesmann, B., and Lange, W.
479 (2005) Cs-rich lithium micas Mn-rich lithian siderophyllite in miarolitic NYF
480 pegmatites of the Königshain granite, Lausitz, Germany. Neues Jahrbuch fur
481 Mineralogie, Abhandlungen, 182, 81–93.
482 Foster, M.D. (1960) Interpretation of the composition of lithium micas. Geological
483 Survey Professional Paper, 354(E), 115–147.
484 Gao, X., Zhou, Z., Breiter, K., Ouyang, H., and Liu, J. (2019) Ore-formation mechanism
485 of the Weilasituo tin–polymetallic deposit, NE China: Constraints from bulk-rock
486 and mica chemistry, He–Ar isotopes, and Re–Os dating. Ore Geology Reviews, 109,
487 163–183.
488 Garate-Olave, I., Roda-Robles, E., Gil-Crespo, P.P., and Pesquera, A. (2018) Mica and

feldspar as indicators of the evolution of a highly evolved granite-pegmatite system in the Tres Arroyos area (Central Iberian Zone, Spain). Journal of Iberian Geology, 44, 375–403.

Gomes, M.E.P., and Neiva, A.M.R. (2005) Geochemistry of granitoids and their minerals from Rebordelo-Agrochão area, northern Portugal. Lithos, 81, 235–254.

Gruber, Paul W., Pablo A. Medina, Gregory A. Keoleian, Stephen E. Kesler, Mark P. Everson, and Timothy J. Wallington (2011) Global Lithium Availability: A Constraint for Electric Vehicles? Journal of Industrial Ecology, 15(4), 1–16.

Henderson, C.M.B., Martin, J.S., and Mason, R.A. (1989) Compositional relations in Li-micas from S.W. England and France: an ion- and electron-microprobe study. Mineralogical Magazine, 53, 427–449.

Jahn, B.M. (2004) The Central Asian Orogenic Belt and growth of the continental crust in the Phanerozoic. Geological Society, London, Special Publications, 226(1), 73–100.

Kalt, A., Schreyer, W., Ludwig, T., Prowatke, S., Bernhardt, H.J., and Ertl, A. (2001) Complete solid solution between magnesian schorl and lithian excess-boron olenite in a pegmatite from the Koralpe (eastern Alps, Austria). European Journal of Mineralogy, 13, 1191–1205.

Kesler, S.E., Gruber, P.W., Medina, P.A., Keoleian, G.A., Everson, M.P., and Wallington, T.J. (2012) Global lithium resources: Relative importance of pegmatite, brine and other deposits. Ore Geology Reviews, 48, 55–69.

Legros, H., Marignac, C., Mercadier, J., Cuney, M., Richard, A., Wang, R.C., Charles, N.,

510 and Lespinasse, M.Y. (2016) Detailed paragenesis and Li-mica compositions as
511 recorders of the magmatic-hydrothermal evolution of the Maoping W-Sn deposit
512 (Jiangxi, China). Lithos, 264, 108–124.

513 Li, J., Huang, X.L., He, P.L., Li, W.X., Yu, Y., and Chen, L.L.(2015) In situ analyses of
514 micas in the Yashan granite, South China: Constraints on magmatic and
515 hydrothermal evolutions of W and Ta-Nb bearing granites. Ore Geology Reviews,
516 65, 793–810.

517 Li, B.Y., Jiang, D.W., Fu, X., Wang, L., Gao, S.Q., Fan, Z.Y., Wang, K.X., and Huge, J.T.
518 (2018) Geological characteristics and prospecting significance of Weilasituo Li
519 polymetallic deposit, Inner Mongolia. Mineral Exploration, 9(6), 1185–1191 (in
520 Chinese).

521 Linnen, R.L., Van Lichtervelde, M., and Černý, P. (2012) Granitic pegmatites as sources
522 of strategic metals. Elements, 8, 275–280.

523 Lu, L., Qin, Y., Zhang, K.J., Han, C.Y., Wei, T., Li, Z.F., Qu, Z.H. (2020) Provenance and
524 tectonic settings of the Late Paleozoic sandstones in central Inner Mongolia, NE
525 China: Constraints on the evolution of the southeastern Central Asian Orogenic Belt.
526 Gondwana Research, 77, 111–135.

527 Martin, G., Schneider, A., Voigt, W., and Bertau, M. (2017) Lithium extraction from the
528 mineral zinnwaldite: Part II: Lithium carbonate recovery by direct carbonation of
529 sintered zinnwaldite concentrate. Minerals Engineering, 110, 75–81.

530 Martins, T., Roda-Robles, E., Lima, A., and De Parseval, P. (2012) Geochemistry and

evolution of micas in the Barroso-Alvão pegmatite field, Northern Portugal. Canadian Mineralogist, 50, 1117–1129.

Mohamed, F.H., Abdalla, H.M., and Helba, H. (1999) Chemistry of micas in rare-metal granitoids and associated rocks, eastern desert, egypt. International Geology Review, 41, 932–948.

Monier, G., and Robert, J.L. (1986) Evolution of the miscibility gap between muscovite and biotite solid solutions with increasing lithium content: an experimental study in the system K_2O-Li_2O-MgO-FeO-Al_2O_3-SiO_2-H_2O-HF at 600°C, 2 kbar P_{H2O}: comparison with natural lithium micas. Mineralogical Magazine, 50, 641–651.

Naumov, A.V., Naumova, M.A. (2010) Modern state of the world lithium market. Russ. J. Non-Ferrous Metals, 51(4), 324–330.

Neiva, A.M.R. (1980) Chlorite and biotite from contact metamorphism of phyllite and metagraywacke by granite, aplite-pegmatite and quartz veins. Chemical Geology, 29, 49–71.

Neiva, A.M.R. (2013) Micas, feldspars and columbite-tantalite minerals from the zoned granitic lepidolite-subtype pegmatite at Namivo, Alto Ligonha, Mozambique. European Journal of Mineralogy, 25, 967–985.

Neiva, A.M.R., Gomes, M.E.P., Ramos, J.M.F., and Silva, P.B. (2008) Geochemistry of granitic aplite-pegmatite sills and their minerals from Arcozelo da Serra area (Gouveia, central Portugal). European Journal of Mineralogy, 20, 465–485.

Qian, X.Y., Zhang, Z.C., Chen, Y., Yu, H.F., Luo, Z.W., Yang, J.F. (2017) Geochronology

552 and geochemistry of early Paleozoic igneous rocks in Zhurihe area, Inner Mongolia
553 and their tectonic significance. Earth Science, 42(9), 1472–1494 (in Chinese).
554 Rentsch, L., Martin, G., Bertau, M., and Höck, M. (2018) Lithium Extracting from
555 Zinnwaldite: Economical Comparison of an Adapted Spodumene and a
556 Direct-Carbonation Process. Chemical Engineering and Technology, 41, 975–982.
557 Rieder, M., Cavazzini, G., D'Yakonov, Y. S., Frank-Kamenetskii, V. A., Gottardi, G.,
558 Guggenheim, S., Koval, P.V., Müller, G., Neiva, A.M.R., Radoslovich, E.W., and
559 others (1999) Nomenclature of the micas. Mineralogical Magazine, 63, 267–279.
560 Roda, E., Keller, P., Pesquera, A., and Fontan, F. (2007) Micas of the muscovite–
561 lepidolite series from Karibib pegmatites, Namibia. Mineralogical Magazine, 71,
562 41–62.
563 Roda-Robles, E., Pesquera, A., Gil-Crespo, P.P., Torres-Ruiz, J., and De Parseval, P.
564 (2006) Mineralogy and geochemistry of micas from the Pinilla de Fermoselle
565 pegmatite (Zamora, Spain). European Journal of Mineralogy, 18, 369–377.
566 Roda-Robles, E., Pesquera, A., Gil-Crespo, P., and Torres-Ruiz, J. (2012) From granite to
567 highly evolved pegmatite: A case study of the Pinilla de Fermoselle
568 granite-pegmatite system (Zamora, Spain). Lithos, 153, 192–207.
569 Roda-Robles, E., Villaseca, C., Pesquera, A., Gil-Crespo, P.P., Vieira, R., Lima, A., and
570 Garate-Olave, I. (2018) Petrogenetic relationships between Variscan granitoids and
571 Li-(F-P)-rich aplite-pegmatites in the Central Iberian Zone: Geological and
572 geochemical constraints and implications for other regions from the European

573 Variscides. Ore Geology Reviews, 95, 408–430.

574 Silva, M.M.V.G., and Neiva, A.M.R. (1990) Geochemistry of the granites and their
575 minerals from Paredes da Beira-Penedono, northern Portugal. Chemical Geology, 85,
576 147–170.

577 Stone, M., Exley, C.S., and George, M.C. (1988) Compositions of trioctahedral micas in
578 the Cornubian batholith. Mineralogical Magazine, 52, 175–192.

579 Thiergärtner, H. (2010) Can the Li_2O content of mica really be calculated from its main
580 chemical components? Zeitschrift fur geologische Wissenschaften, 38, 195–205.

581 Tian, J., Xu, L., Wu, H., Fang, S., Deng, W., Peng, T., Sun, W., and Hu, Y. (2018) A novel
582 approach for flotation recovery of spodumene, mica and feldspar from a lithium
583 pegmatite ore. Journal of Cleaner Production, 174, 625–633.

584 Tindle, A.G., and Webb, P.C. (1990) Estimation of lithium contents in trioctahedral micas
585 using microprobe data: application to micas from granitic rocks. European Journal
586 of Mineralogy, 2, 595–610.

587 Tischendorf, G. (1999) The Correlation Between Lithium and Magnesium in
588 Trioctahedral Micas: Improved Equations for Li_2O Estimation from MgO Data.
589 Mineralogical Magazine, 63, 57–74.

590 Tischendorf, G., Gottesmann, B., Förster, H.-J., and Trumbull, R.B. (1997) On Li-bearing
591 micas: estimating Li from electron microprobe analyses and an improved diagram
592 for graphical representation. Mineralogical Magazine, 61, 809–834.

593 Tischendorf, G., Förster, H.-J., and Gottesmann, B. (2001) Minor- and trace-element

composition of trioctahedral micas: a review. Mineralogical Magazine, 65(2), 249–276.

Van Lichtervelde, M., Grégoire, M., Linnen, R.L., Béziat, D., and Salvi, S. (2008) Trace element geochemistry by laser ablation ICP-MS of micas associated with Ta mineralization in the Tanco pegmatite, Manitoba, Canada. Contributions to Mineralogy and Petrology, 155, 791–806.

Vieira, R., Roda-Robles, E., Pesquera, A., and Lima, A. (2011) Chemical variation and significance of micas from the Fregeneda-Almendra pegmatitic field (Central-Iberian Zone, Spain and Portugal). American Mineralogist, 96, 637–645.

Wang, F., Bagas, L., Jiang, S., and Liu, Y. (2017) Geological, geochemical, and geochronological characteristics of Weilasituo Sn-polymetal deposit, Inner Mongolia, China. Ore Geology Reviews, 80, 1206–1229.

Xie, L., Wang, R.C., Groat, L.A., Zhu, J.C., Huang, F.F., and Cempírek, J. (2015) A combined EMPA and LA-ICP-MS study of Li-bearing mica and Sn-Ti oxide minerals from the Qiguling topaz rhyolite (Qitianling District, China): The role of fluorine in origin of tin mineralization. Ore Geology Reviews, 65, 779–792.

Xie, L., Wang, Z., Wang, R., Zhu, J., Che, X., Gao, J., and Zhao, X. (2018) Mineralogical constraints on the genesis of W–Nb–Ta mineralization in the Laiziling granite (Xianghualing district, south China). Ore Geology Reviews, 95, 695–712.

Yavuz, F. (2001) LIMICA: A program for estimating Li from electron-microprobe mica analyses and classifying trioctahedral micas in terms of composition and octahedral

site occupancy. Computers and Geosciences, 27, 215–227.

Yin, R., Huang, X.L., Xu, Y.G., Wang, R.C., Wang, H., Yuan, C., Ma, Q., Sun, X.M., and Chen, L.L. (2020) Mineralogical constraints on the magmatic–hydrothermal evolution of rare-elements deposits in the Bailongshan granitic pegmatites, Xinjiang, NW China. Lithos, 352–353, 105208.

Zhou, Q. F., Qin, K. Z., Tang, D. M., Ding, J. G., and Guo, Z. L. (2013) Mineralogy and significance of micas and feldspars from the koktokay no. 3 pegmatitic rare-element deposit, altai. Acta Petrologica Sinica, 29(9), 3004–3022 (in Chinese).

Zou, H., and Hastie, T. (2005) Regularization and variable selection via the elastic net, Journal of the Royal Statistical Society. Series B: Statistical Methodology, 67(2), 301–320.

Other references cited in the supporting information

Akoh, J.U., Ogunleye, P.O., and Ibrahim, A.A. (2015) Geochemical evolution of micas and Sn-, Nb-, Ta- mineralization associated with the rare metal pegmatite in Angwan Doka, central Nigeria. Journal of African Earth Sciences, 112, 24–36.

Alva-Jimenez, T. (2011) Variation in hydrothermal muscovite and chlorite composition in the Highland Valley Porphyry Cu-Mo District, British Columbia, Canada, master's thesis, The University of British Columbia.

634 Araujo, F.P., Martins, L., Pereira, G. de S., and Janasi, V. de A. (2020) Inhandjara topaz
635 leucogranite: A late rare metal-mineralized stock within the A-type Itu batholith, SE
636 Brazil. Journal of South American Earth Sciences, 101, 102623.
637 Barrière, M., and Cotten, J. (1979) Biotites and associated minerals as markers of
638 magmatic fractionation and deuteric equilibration in granites. Contributions to
639 Mineralogy and Petrology, 70(2), 183–192.
640 Bea, F., Pereira, M.D., and Stroh, A. (1994) Mineral/leucosome trace-element partitioning
641 in a peraluminous migmatite (a laser ablation-ICP-MS study). Chemical Geology,
642 117(1–4), 291–312.
643 Bigi, S., and Brigatti, M.F. (1994) Crystal chemistry and microstructures of plutonic
644 biotite. American Mineralogist, 79, 63–72.
645 Breiter, K., Ďurišová, J., Hrstka, T., Korbelová, Z., Vašinová Galiová, M., Müller, A.,
646 Simons, B., Shail, R.K., Williamson, B.J., Davies, J.A. (2018) The transition from
647 granite to banded aplite-pegmatite sheet complexes: An example from Megiliggar
648 Rocks, Tregonning topaz granite, Cornwall. Lithos, 302–303, 370–388.
649 Brigatti, M.F., and Davoli, P. (1990) Crystal-structure refinements of 1M plutonic biotites.
650 American Mineralogist, 75(3–4), 305–313.
651 Campeny, M., Kamenetsky, V.S., Melgarejo, J.C., Mangas, J., Manuel, J., Alfonso, P.,
652 Kamenetsky, M.B., Bambi, A.C.J.M., Gonçalves A.O. (2015) Carbonatitic lavas in
653 Catanda (Kwanza Sul, Angola): Mineralogical and geochemical constraints on the
654 parental melt. Lithos, 232, 1–11.

Černý, P., and Trueman, D.L. (1985) Polylithionite from the rare-metal deposits of the Blachford Lake alkaline complex, N.W.T., Canada. American Mineralogist, 70(11–12), 1127–1134.

Černý, P., Rieder, M., and Povondra, P. (1970) Three polytypes of lepidolite from Czechoslovakia. Lithos, 3, 319–325.

Černý, P., Staněk, Novák, M., Baadsgaard, H., Rieder, M., Ottolini, L., Kavalová, M., and Chapman, R. (1995) Geochemical and structural evolution of micas in the Rožná and Dobrá Voda pegmatites, Czech Republic. Mineralogy and Petrology, 55, 177–201.

Chaudhry, M.N., and Howie, R.A. (1973) Lithium tourmalines from the Meldon aplite, Devonshire, England. Mineralogical Magazine, 39, 289–296.

Codeço, M.S., Weis, P., Trumbull, R.B., Glodny, J., Wiedenbeck, M., and Romer, R.L. (2019) Boron isotope muscovite-tourmaline geothermometry indicates fluid cooling during magmatic-hydrothermal W-Sn ore formation. Economic Geology, 114(1), 153–163.

Codeço, M.S., Weis, P., Trumbull, R.B., van Hinsberg, V., Pinto, F., Lecumberri-Sanchez, P., and Schleicher, A.M. (2020b): Trace element contents in white mica and tourmaline from the Panasqueira W-Sn-Cu deposit (Portugal). GFZ Data Services. https://doi.org/10.5880/GFZ.3.1.2020.002

Cooper, A.F., Paterson, L.A., and Reid, D.L. (1995) Lithium in carbonatites—consequence of an enriched mantle source? Mineralogical Magazine, 59(396), 401–408.

676 Deveaud, S., Millot, R., and Villaros, A. (2015) The genesis of LCT-type granitic
677 pegmatites, as illustrated by lithium isotopes in micas. Chemical Geology, 411, 97–
678 111.
679 du Bray, E.A. (1994) Compositions of micas in peraluminous granitoids of the eastern
680 Arabian shield-Implications for petrogenesis and tectonic setting of highly evolved,
681 rare-metal enriched granites. Contributions to Mineralogy and Petrology, 116(4),
682 381–397.
683 Fabre, C., Boiron, M.C., Dubessy, J., Chabiron, A., Charoy, B., and Martin Crespo, T.
684 (2002) Advances in lithium analysis in solids by means of laser-induced breakdown
685 spectroscopy: An exploratory study. Geochimica et Cosmochimica Acta, 66(8),
686 1401–1407.
687 Fitzpayne, A., Giuliani, A., Hergt, J., Phillips, D., and Janney, P. (2018) New geochemical
688 constraints on the origins of MARID and PIC rocks: Implications for mantle
689 metasomatism and mantle-derived potassic magmatism. Lithos, 318–319, 478–493.
690 Foord, E.E., Černý, P., Jackson, L.L., Sherman, D.M., and Eby, R.K. (1995) Mineralogical
691 and geochemical evolution of micas from miarolitic pegmatites of the anorogenic
692 pikes peak batholith, Colorado. Mineralogy and Petrology, 55(1–3), 1–26.
693 Fritschle, T., Prelević, D., Foley, S.F., and Jacob, D.E. (2013) Petrological characterization
694 of the mantle source of Mediterranean lamproites: Indications from major and trace
695 elements of phlogopite. Chemical Geology, 353, 267–279.

696 Giuliani, A., Phillips, D., Kamenetsky, V.S., and Goemann, K. (2016) Constraints on
697 kimberlite ascent mechanisms revealed by phlogopite compositions in kimberlites
698 and mantle xenoliths. Lithos, 240–243, 189–201.
699 Grew, E.S., Chernosky, J.V., Werding, G., Abraham, K., Marquez, N., and Hinthorne, J.R.
700 (1990) Chemistry of kornerupine and associated minerals, a wet chemical, ion
701 microprobe, and X-ray study emphasizing Li, Be, B and F contents. Journal of
702 Petrology, 31(5), 1025–1070.
703 Grew, E.S., Hiroi, Y., Motoyoshi, Y., Kondo, Y., Jayatileke, S.J.M., and Marquez, N.
704 (1995) Iron-rich kornerupine in sheared pegmatite from the Wanni Complex, at
705 Homagama, Sri Lanka. European Journal of Mineralogy, 7(3), 623–636.
706 Gu, L.X., Zhang, Z.Z., Wu, C.Z., Gou, X.Q., Liao, J.J., and Yang, H. (2011) A topaz- and
707 amazonite-bearing leucogranite pluton in eastern Xinjiang, NW China and its zoning.
708 Journal of Asian Earth Sciences, 42(5), 885–902.
709 Hawthorne, F.C., Sokolova, E., Agakhanov, A.A., Pautov, L.A., and Karpenko, V.Y.U.
710 (2019) The crystal structure of polylithionite-1M from Darai-Pioz, Tajikistan: The
711 role of short-range order in driving symmetry reduction in 1M Li-rich mica. Canadian
712 Mineralogist, 57(4), 519–528.
713 Heinrich, E.W. (1967) Micas of the brown Derby pegmatites, Cunnison County, Colorado.
714 The American Mineralogist, 52, 1110–1121.

715 Hou, J.L., Li, J.K., Wang, D.H., Chen, Z.Y., Dai, H.Z., and Liu, L.J. (2017) Geochemical
716 Characteristics and Geological Significance of Biotite in Granite Bodies of Jiajika
717 Lithium Mine, Sichuan Province. Gold Science and Technology, 25(6), 1–8.
718 Jacob, D.E., Viljoen, K.S., and Grassineau, N.V. (2009) Eclogite xenoliths from
719 Kimberley, South Africa - A case study of mantle metasomatism in eclogites. Lithos,
720 112, 1002–1013.
721 Jolliff, B.L., Papike, J.J., and Shearer, C.K. (1987) Fractionation trends in mica and
722 tourmaline as indicators of pegmatite internal evolution: Bob Ingersoll pegmatite,
723 Black Hills, South Dakota. Geochimica et Cosmochimica Acta, 51(3), 519–534.
724 Li, J., Huang, X.L., Wei, G.J., Liu, Y., Ma, J.L., Han, L., and He, P.L. (2018) Lithium
725 isotope fractionation during magmatic differentiation and hydrothermal processes in
726 rare-metal granites. Geochimica et Cosmochimica Acta, 240, 64–79.
727 Liu, C., Wang, R.C., Wu, F.Y., Xie, L., Liu, X.C., Li, X.K., Yang, L., Li, X.J. (2020)
728 Spodumene pegmatites from the Pusila pluton in the higher Himalaya, South Tibet:
729 Lithium mineralization in a highly fractionated leucogranite batholith. Lithos, 358–
730 359, 105421.
731 Liu, Y., Xie, L., Wang, R.C., Hu, H., Che, X.D., Tian, E.N., and Xiang, L. (2018)
732 Comparative study of petrogenesis and mineralization characteristics of
733 Nb-Ta-bearing and W-bearing granite in the Dahutang deposit, Northern Jiangxi
734 Province. Acta Geologica Sinica, 92(10), 2120–2137 (in Chinese).

735 Luecke, W. (1981) Lithium pegmatites in the Leinster Granite (southeast Ireland).
736 Chemical Geology, 34(3–4), 195–233.
737 Miyawaki, R., Shimazaki, H., Shigeoka, M., Yokoyama, K., Matsubara, S., and Yurimoto,
738 H. (2011) Yangzhumingite, $KMg_{2.5}Si_4O_{10}F_2$, a new mineral in the mica group from
739 Bayan Obo, Inner Mongolia, China. European Journal of Mineralogy, 23(3), 467–
740 473.
741 Monier, G., Charoy, B., Cuney, M., Ohnenstetter, D. and Robert, J.L. (1987) Évolution
742 spatiale et temporellede la composition des micas du granite albitique à
743 topaze-lépidolite de Beauvoir. Géologie de la France, 2–3, 179–188.
744 Müller, G. (1966) Die Beziehungen zwischen der chemischen Zusammensetzung,
745 Lichtbrechung und Dichte einiger koexistierender Biotite, Muskowite und Chlorite
746 aus granitischen Tiefengesteinen. Contributions to Mineralogy and Petrology, 12(2),
747 173–191.
748 Neiva, A.M.R., and Gomes, M.E.P. (1991) Geochemistry of the granitoid rocks and their
749 minerals from Lixa do Alvão-Alfarela de Jales-Tourencinho (Vila Pouca de Aguiar,
750 northern Portugal). Chemical Geology, 89(3–4), 305–327.
751 Neiva, A.M.R., Silva, M.M.V.G., Gomes, M.E.P., and Campos, T.F.C. (2002)
752 Geochemistry of coexisting biotite and muscovite of Portuguese peraluminous
753 granitic differentiation series. Chemie Der Erde, 62(3), 197–215.

754 Pérez-Soba, C., and Villaseca, C. (2019) Li-Na-metasomatism related to I-type granite
755 magmatism: A case study of the highly fractionated La Pedriza pluton (Iberian
756 Variscan belt). Lithos, 344–345, 159–174.
757 Pesquera, A., Torres-Ruiz, J., Gil-Crespo, P.P., and Velilla, N. (1999) Chemistry and
758 genetic implications of tourmaline and Li-F-Cs micas from the Valdeflores area
759 (Caceres, Spain). American Mineralogist, 84(1–2), 55–69.
760 Petrík, I., Čík, Š., Miglierini, M., Vaculovič, T., Dianiška, I., and Ozdín, D. (2014) Alpine
761 oxidation of lithium micas in Permian S-type granites (Gemeric unit, Western
762 Carpathians, Slovakia). Mineralogical Magazine, 78(3), 507–533.
763 Qu, K., Sima, X., Li, G., Fan, G., Shen, G., Liu, X., Xiao, Z., Guo, H., Qiu, L., and Wang,
764 Y. (2020) Fluorluanshiweiite, $KLiAl_{1.5}\square_{0.5}(Si_{3.5}Al_{0.5})O_{10}F_2$, a new mineral of the mica
765 group from the Nanyangshan LCT pegmatite deposit, North Qinling Orogen, China.
766 Minerals, 10(2), 1–12.
767 Rieder, M., Huka, M., Kučerová, D., Minařík, L., Obermajer, J., and Povondra, P. (1970)
768 Chemical composition and physical properties of lithium-iron micas from the Krušné
769 hory Mts. (Erzgebirge) - Part A: Chemical composition. Contributions to Mineralogy
770 and Petrology, 27(2), 131–158.
771 Rieder, M., Haapala, I., and Povondra, P. (1996) Mineralogy of dark mica from the Wiborg
772 rapakivi batholith, southeastern Finland. European Journal of Mineralogy, 8(3), 593–
773 606.

774 Rinaldi, R., Černý, P., and Ferguson, R.B. (1972) The Tanco pegmatite at Bernic Lake,
775 Manitoba. VI. Lithium-Rubidium-Cesium micas. Canadian Mineralogist, 11, 690–
776 707.
777 Roda, E., Pesquera, A., and Velasco, F. (1995) Micas of the muscovite-lepidolite series
778 from the Fregeneda pegmatites (Salamanca, Spain). Mineralogy and Petrology, 55,
779 145–157.
780 Rosing-Schow, N., Müller, A., and Friis, H. (2018) A comparison of the mica
781 geochemistry of the pegmatite fields in southern norway. Canadian Mineralogist,
782 56(4), 463–488.
783 Savage, D., Cave, M.R., Milodowski, A.E., and George, I. (1987) Hydrothermal alteration
784 of granite by meteoric fluid: an example from the Carnmenellis Granite, United
785 Kingdom. Contributions to Mineralogy and Petrology, 96, 391–405.
786 Scordari, F., Dyar, M.D., Schingaro, E., Lacalamita, M., and Ottolini, L. (2010) XRD,
787 micro-XANES, EMPA, and SIMS investigation on phlogopite single crystals from
788 Mt. Vulture (Italy). American Mineralogist, 95(11–12), 1657–1670.
789 Sharygin, V.V. (2017) Tainiolite From Chuktukon Carbonatite Massif, Chadobets. Paper
790 presented at 34th International conference “Magmatism of the Earth and related
791 strategic metal deposits”, Vernadsky Institute of Geochemistry and Anlytical
792 Chemistry of Russian Academy of Sciences, Miass.

793 Shearer, C.K., Papike, J.J., Simon, S.B., and Laul, J.C. (1986) Pegmatite-wall-rock
794 interactions, Black Hills, South Dakota: interaction between pegmatite-derived fluids
795 and quartz-mica schist wall-rock. American Mineralogist, 71(3–4), 518–539.
796 Simons, B., Andersen, J.C.Ø., Shail, R.K., and Jenner, F.E. (2017) Fractionation of Li, Be,
797 Ga, Nb, Ta, In, Sn, Sb, W and Bi in the peraluminous Early Permian Variscan granites
798 of the Cornubian Batholith: Precursor processes to magmatic-hydrothermal
799 mineralisation. Lithos, 278–281, 491–512.
800 Sun, K., Chen, B., and Deng, J. (2019) Biotite in highly evolved granites from the Shimensi
801 W–Cu–Mo polymetallic ore deposit, China: Insights into magma source and
802 evolution. Lithos, 350–351, 105245.
803 Taylor, R.P. (1992) Petrological and geochemical characterisitcs of the pleasant ridge
804 zinnwaldite-topaz granite, southern New Brunswick, and comparisons with other
805 topaz-bearing felsic rocks. Canadian Mineralogist, 30, 895–921.
806 Villaros, A., and Pichavant, M. (2019) Mica-liquid trace elements partitioning and the
807 granite-pegmatite connection: The St-Sylvestre complex (Western French Massif
808 Central). Chemical Geology, 528, 119265.
809 Wang, Z.J., Xie, L., Wang, R.C., Zhu, J.C., Che, X.D., and Zhao, X. (2018) The
810 Petrogenesis and Mineralization of the Laiziling Greisen, Xianghualing District,
811 Hunan Province, South China. Geological Journal of China Universities, 24(4), 467–
812 480.

Wei, B., Wang, C.Y., Zhao, Z., and Bao, H. (2020) Columbite-group minerals and mica of peraluminous granite record the magmatic-hydrothermal processes that formed the Zhaojinggou Ta-Nb deposit in the North China Craton. Lithos, 370–371, 105648.

Weidendorfer, D., Schmidt, M.W., and Mattsson, H.B. (2016) Fractional crystallization of Si-undersaturated alkaline magmas leading to unmixing of carbonatites on Brava Island (Cape Verde) and a general model of carbonatite genesis in alkaline magma suites. Contributions to Mineralogy and Petrology, 171, 43.

Whalen, J.B. (1985) Geochemistry of an Island-arc plutonic suite: The Uasilau-Yau Yau intrusive complex, New Britain, P.N.G. Journal of Petrology, 26(3), 603–632.

Xie, L., Wang, R.C., Che, X.D., Huang, F.F., Erdmann, S., and Zhang, W.L. (2016) Tracking magmatic and hydrothermal Nb-Ta-W-Sn fractionation using mineral textures and composition: A case study from the late Cretaceous Jiepailing ore district in the Nanling Range in South China. Ore Geology Reviews, 78, 300–321.

Xie, L., Liu, Y., Wang, R., Hu, H., Che, X., and Xiang, L. (2019) Li–Nb–Ta mineralization in the Jurassic Yifeng granite-aplite intrusion within the Neoproterozoic Jiuling batholith, south China: A fluid-rich and quenching ore-forming process. Journal of Asian Earth Sciences, 185, 104047.

Xie, L., Tao, X., Wang, R., Wu, F., Liu, C., Liu, X., Li, X., and Zhang, R. (2020) Highly fractionated leucogranites in the eastern Himalayan Cuonadong dome and related magmatic Be–Nb–Ta and hydrothermal Be–W–Sn mineralization. Lithos, 354–355, 105286.

834 Xing, F.M., and Xu, X. (1991). Biotite in Mesozoic intermediate-acidity intrusions from
835 south Anhui and its tectonic significance. Mineralogy and Petrology, 11(1), 29–36.
836 Xue, R., Wang, R.C., Chen, G.H., Che, X.D., Xie, L., and Zhu, Z.Y. (2019) Compositional
837 constraints of mica and wolframite on hydrothermal ore-forming process of the
838 Songshugang Ta-Sn deposit, northeastern Jiangxi. Acta Petrologica et Mineralogica,
839 38(4), 507–520 .
840 Yang, P., and Rivers, T. (2000) Trace element partitioning between coexisting biotite and
841 muscovite from metamorphic rocks, Western Labrador: Structural, compositional and
842 thermal controls. Geochimica et Cosmochimica Acta, 64(8), 1451–1472.
843 Zhou, Q.F., Qin, K.Z., Tang, D.M., Ding, J.G., and Guo, Z.L. (2013) Mineralogy and
844 significance of micas and feldspars from the koktokay no. 3 pegmatitic rare-element
845 deposit, altai. Acta Petrologica Sinica, 29(9), 3004–3022 (in Chinese) .
846
847
848
849
850
851
852
853
854

This is the peer-reviewed, final accepted version for American Mineralogist, published by the Mineralogical Society of America.
The published version is subject to change. Cite as Authors (Year) Title. American Mineralogist, in press.
DOI: https://doi.org/10.2138/am-2022-8029. http://www.minsocam.org/

855

TABLES

TABLE 1. R^2 and RMSE values for training and test sets by the MPR method

No.	Training set		Test set	
	R^2	RMSE (wt%)	R^2	RMSE (wt%)
Dataset1				
1	0.95	0.31	0.94	0.39
2	0.95	0.32	0.94	0.37
3	0.95	0.32	0.95	0.35
4	0.95	0.32	0.92	0.40
5	0.96	0.30	0.91	0.44
6	0.95	0.32	0.94	0.36
7	0.95	0.31	0.93	0.41
8	0.95	0.32	0.89	0.48
9	0.95	0.32	0.93	0.39
10	0.95	0.32	0.95	0.36
11	0.95	0.32	0.90	0.47
12	0.95	0.32	0.92	0.42
13	0.96	0.30	0.87	0.54
14	0.95	0.32	0.94	0.36
15	0.95	0.32	0.93	0.39
16	0.95	0.30	0.93	0.43
17	0.96	0.31	0.90	0.46
18	0.96	0.31	0.88	0.50
19	0.95	0.32	0.91	0.45
20	0.93	0.38	0.92	0.44
Dataset2				
1	0.96	0.22	0.95	0.26
2	0.97	0.21	0.95	0.25
3	0.97	0.21	0.94	0.24
4	0.97	0.19	0.94	0.31
5	0.97	0.21	0.94	0.28
6	0.97	0.20	0.93	0.29
7	0.97	0.20	0.93	0.27
8	0.97	0.20	0.94	0.30
9	0.97	0.20	0.93	0.26
10	0.96	0.20	0.94	0.29
11	0.97	0.20	0.92	0.30
12	0.97	0.19	0.93	0.31

13	0.97	0.21	0.94	0.27
14	0.96	0.21	0.96	0.26
15	0.97	0.19	0.92	0.33
16	0.96	0.22	0.96	0.22
17	0.97	0.20	0.93	0.28
18	0.97	0.20	0.93	0.30
19	0.97	0.21	0.94	0.27
20	0.97	0.20	0.93	0.31

Note: n = 20 random splitting for each data model.

856

TABLE 2. Summary of published empirical equations for estimating Li_2O contents in tri- and di-octahedral micas

Equations	Analyzed number	Goodness of fit (R^2)	Range of validity (wt%)
$Li_2O^a = (0.287\times SiO_2)–9.552$	400	0.90	Trioctahedral micas with MgO <8
$Li_2O^{b,c} = (0.289\times SiO_2)–9.658$	232	0.91	Trioctahedral micas with Li_2O >0.6, MgO <3, SiO_2 >34
$Li_2O^c = [2.7/(0.35+MgO)]–0.13$	434	0.88	Trioctahedral micas with MgO = 0.01 to 20
$Li_2O^c = 0.237\times F^{1.544}$	501	0.85	Trioctahedral micas with F = 0.1–9
$Li_2O^c = 0.177\times F^{1.642}$	439	0.91	Trioctahedral micas excluding aplites and pegmatites
$Li_2O^c = 0.3935\times F^{1.326}$	199	0.84	Dioctahedral mica
$Li_2O^b = 2.1/(0.356+MgO)–0.088$	870	0.91	Normal group of trioctahedral

This is the peer-reviewed, final accepted version for American Mineralogist, published by the Mineralogical Society of America.
The published version is subject to change. Cite as Authors (Year) Title. American Mineralogist, in press.
DOI: https://doi.org/10.2138/am-2022-8029. http://www.minsocam.org/

			micas with MgO = 0–24.5
Li_2O[b] = 98/(12.8+MgO)–0.3	22	0.94	High Li-Mg, Al-poor group of trioctahedral micas with MgO = 0–29.0
Li_2O[b] = 50.3/(6.5+MgO)–1.54	84	0.90	High Li-Mg, Al-rich group of trioctahedral micas with MgO = 0–26.2
Li_2O[d] = 0.7200×F–0.6120	9	0.97	—
Li_2O[e] = 0.7823×F+0.0131	42	0.92	—
Li_2O[f] = 0.5387×F–0.1205	11	0.97	—
Li_2O[g] = 0.5808×F–0.0669	—	—	—

[a]Tindle and Webb (1990). [b]Tischendorf (1999). [c]Tischendorf et al. (1997). [d] Roda et al. (2007). [e]Van Lichtervelde et al. (2008). [f]Vieira et al. (2011). [g]Martins et al. (2012).

857

TABLE 3. R^2 and RMSE values for the best-performed MPR model and published empirical equations

Equations	Dataset1			Dataset2		
	Number	R^2	RMSE (wt%)	Number	R^2	RMSE (wt%)
MPR[a]	638	0.95	0.35	416	0.96	0.22
Li_2O[b]=(0.287×SiO_2)–9.552	164	0.82	0.73	51	0.84	0.68

This is the peer-reviewed, final accepted version for American Mineralogist, published by the Mineralogical Society of America.
The published version is subject to change. Cite as Authors (Year) Title. American Mineralogist, in press.
DOI: https://doi.org/10.2138/am-2022-8029. http://www.minsocam.org/

$Li_2O^{c,d}=(0.289\times SiO_2)-9.658$	124	0.68	0.88	33	0.52	0.78
$Li_2O^{d}=[2.7/(0.35+MgO)]-0.13$	220	0.53	1.86	80	0.57	1.30
$Li_2O^{d}=0.237\times F^{1.544}$	311	0.82	0.95	168	0.80	0.74
$Li_2O^{d}=0.177\times F^{1.642}$	394	0.78	0.85	143	0.78	0.81
$Li_2O^{d}=0.3935\times F^{1.326}$	306	0.51	0.40	242	0.53	0.33

[a]this study. [b]Tindle and Webb (1990). [c]Tischendorf (1999). [d]Tischendorf et al. (1997).

FIGURE CAPTIONS

FIGURE 1. Compiled mica compositions from dataset 1 **(a)** and dataset 2 **(b)** plotted in the classification diagram of Tischendorf et al. (1997). Mineral abbreviations: lepidomelane (Lpm), protolithionite (Prl), siderophyllite (Sdr), biotite (Bt), phlogopite (Phl), lepidolite (Lpd), zinnwaldite (Znw), phengite (Ph), muscovite (Ms), and taeniolite (Tae).

FIGURE 2. Predicted vs. measured Li_2O contents for the best-performed dataset 1 **(a)** and dataset 2 **(b)** models using the MPR method.

FIGURE 3. Error distributions for the test set of the best-performed dataset 1 **(a)** and dataset 2 **(b)** models.

FIGURE 4. Predicted vs. measured Li_2O contents for the published empirical equations using the test set of the best-performed dataset 1 model. The green diamonds refer to predicted results of the MPR method. The orange crosses refer to predicted results of micas that match the recommended ranges of validity for the empirical equations, and the

873 blue crosses are those falling outside the ranges of validity.

874 **FIGURE 5.** Predicted vs. measured Li_2O contents for the published empirical equations
875 using the test set of the best-performed dataset 2 model. The symbols are the same as
876 those in figure 4.

877 **FIGURE 6.** Li_2O vs. F diagrams for di- and tri-octahedral micas in dataset 2.

878 **FIGURE 7. (a)** Location of central Inner Mongolia (modified after Jahn 2004). **(b)**
879 Geological sketch map of central Inner Mongolia showing lithological and tectonic units
880 (modified after Lu et al. 2020 and Qian et al. 2017). Abbreviations: NCC–North China
881 craton. TC–Tarim craton. WLST–Weilasituo. SHY–Shihuiyao. BYG–Bayangen. JBS–
882 Jiabusi. SMACM–South Mongolia–Uliastai active continental margin. HOAC–
883 Hegenshan ophiolite accretionary complex. BAAC–Baolidao arc accretionary complex.
884 SOAC–Solonker ophiolite accretionary complex. OAC–Ondor Sum subduction
885 accretionary complex. BA–Bainaimiao arc.

886 **FIGURE 8.** Predicted vs. measured Li_2O contents for the MPR method and empirical
887 equations on micas from Gao et al. (2019).

888 **FIGURE 9.** Classification diagram of Tischendorf et al. (1997) illustrating mica
889 compositions of rock samples from the Weilasituo, Jiabusi, Shihuiyao and Bayangen
890 areas. Mineral abbreviations are the same as those in figure 1.

891 **FIGURE 10.** Photomicrographs (polarized plane), BSE images and Li (apfu) profiles of
892 representative mica grains from the Jiabusi area. Mineral abbreviations: albite (Ab),
893 lepidolite (Lpd), elbaite (Elb), zinnwaldite (Znw), fluorite (Fl), topaz (Tpz).

This is the peer-reviewed, final accepted version for American Mineralogist, published by the Mineralogical Society of America.
The published version is subject to change. Cite as Authors (Year) Title. American Mineralogist, in press.
DOI: https://doi.org/10.2138/am-2022-8029. http://www.minsocam.org/

Figure 1

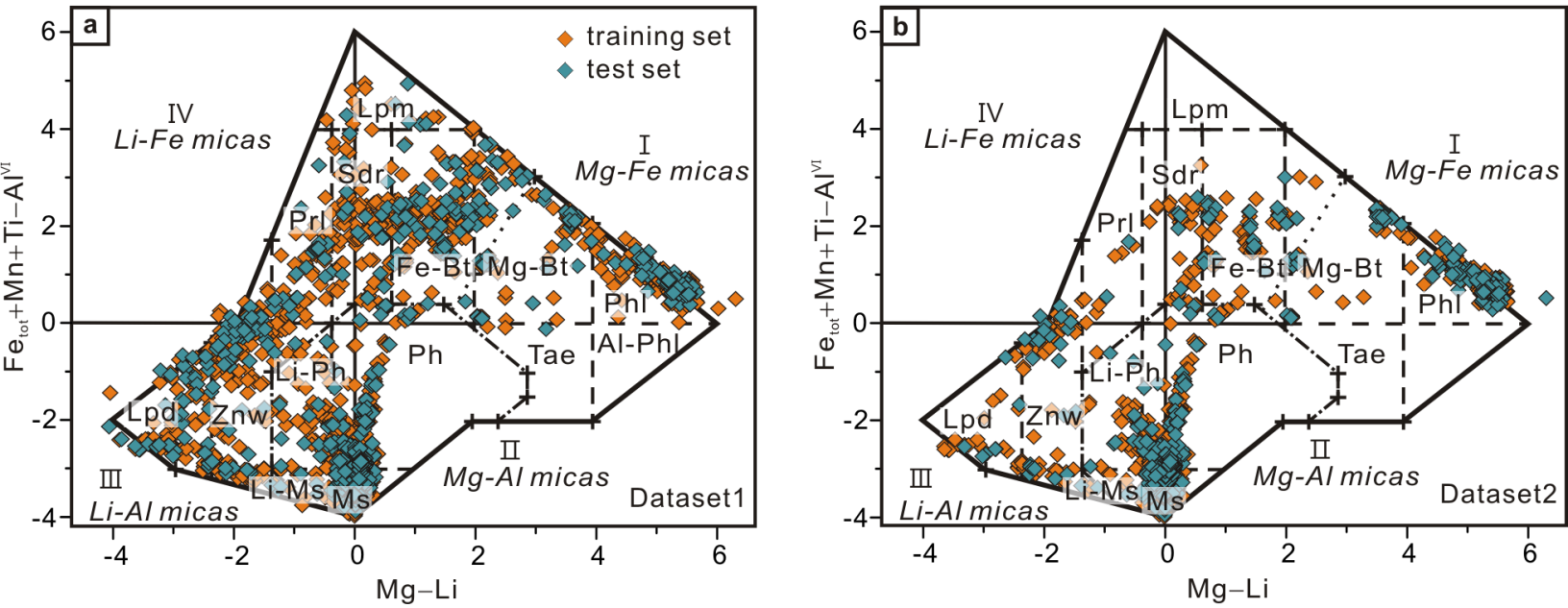

This is the peer-reviewed, final accepted version for American Mineralogist, published by the Mineralogical Society of America.
The published version is subject to change. Cite as Authors (Year) Title. American Mineralogist, in press.
DOI: https://doi.org/10.2138/am-2022-8029. http://www.minsocam.org/

Figure 2

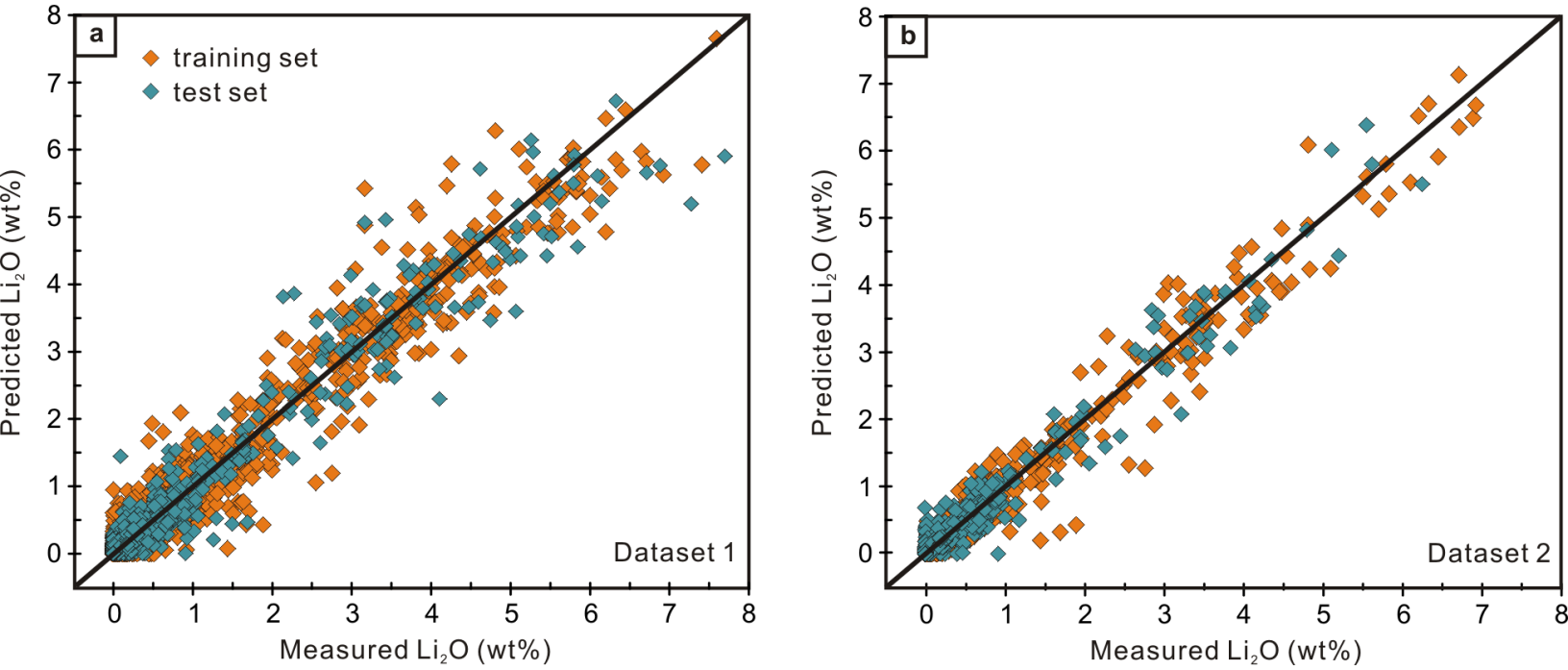

This is the peer-reviewed, final accepted version for American Mineralogist, published by the Mineralogical Society of America.
The published version is subject to change. Cite as Authors (Year) Title. American Mineralogist, in press.
DOI: https://doi.org/10.2138/am-2022-8029. http://www.minsocam.org/

Figure 3

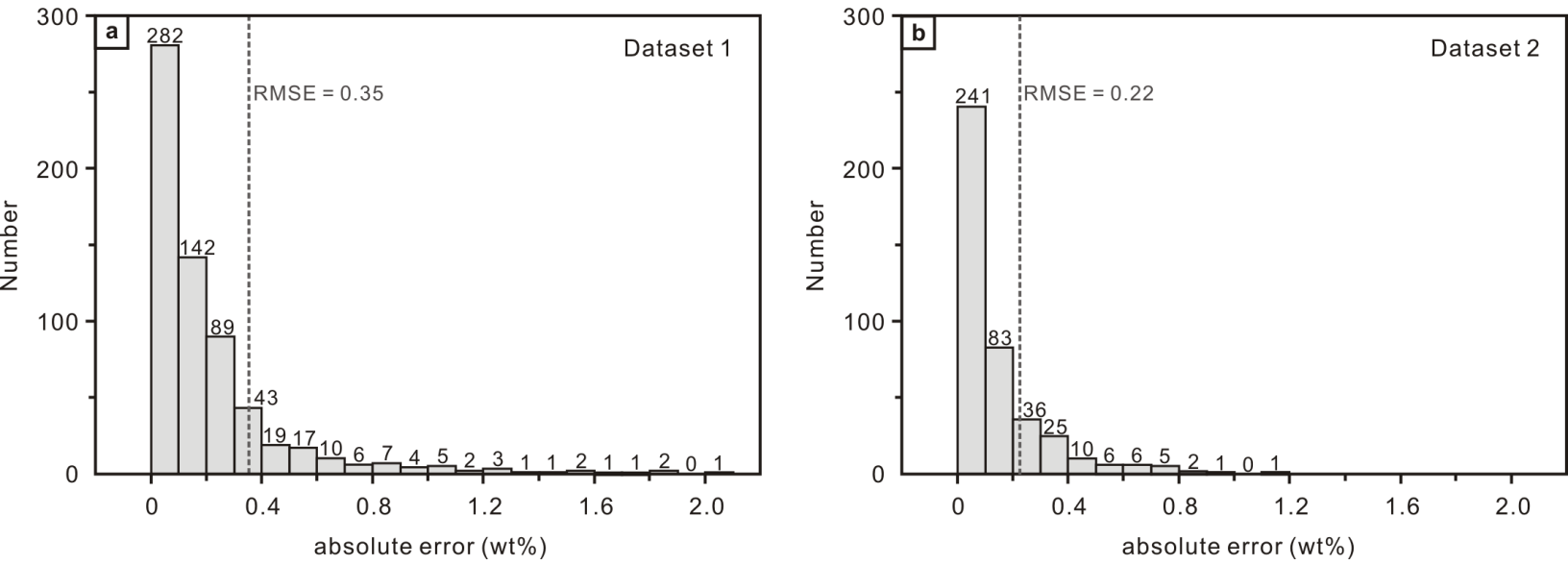

This is the peer-reviewed, final accepted version for American Mineralogist, published by the Mineralogical Society of America.
The published version is subject to change. Cite as Authors (Year) Title. American Mineralogist, in press.
DOI: https://doi.org/10.2138/am-2022-8029. http://www.minsocam.org/

Figure 4

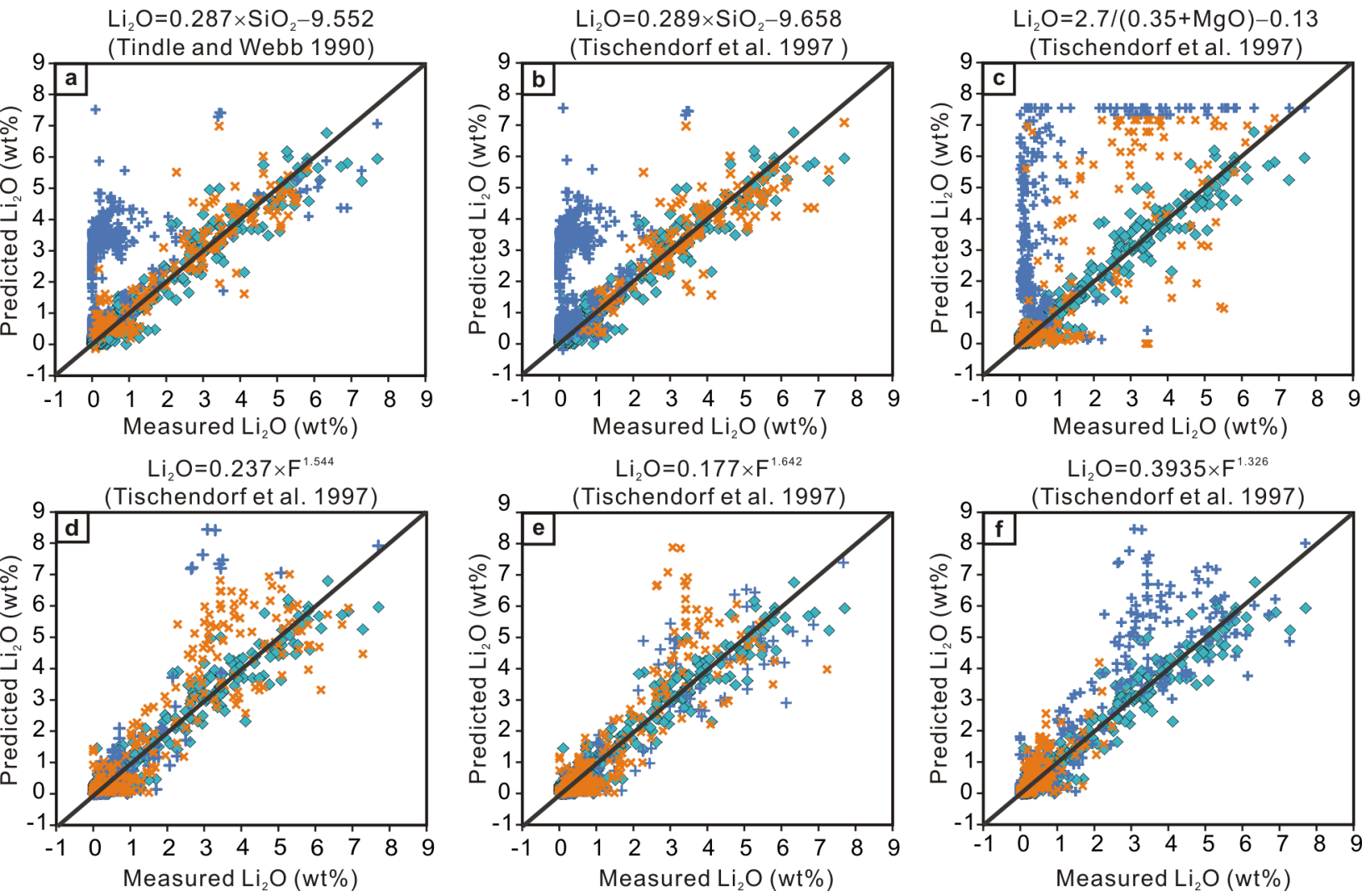

This is the peer-reviewed, final accepted version for American Mineralogist, published by the Mineralogical Society of America.
The published version is subject to change. Cite as Authors (Year) Title. American Mineralogist, in press.
DOI: https://doi.org/10.2138/am-2022-8029. http://www.minsocam.org/

Figure 5

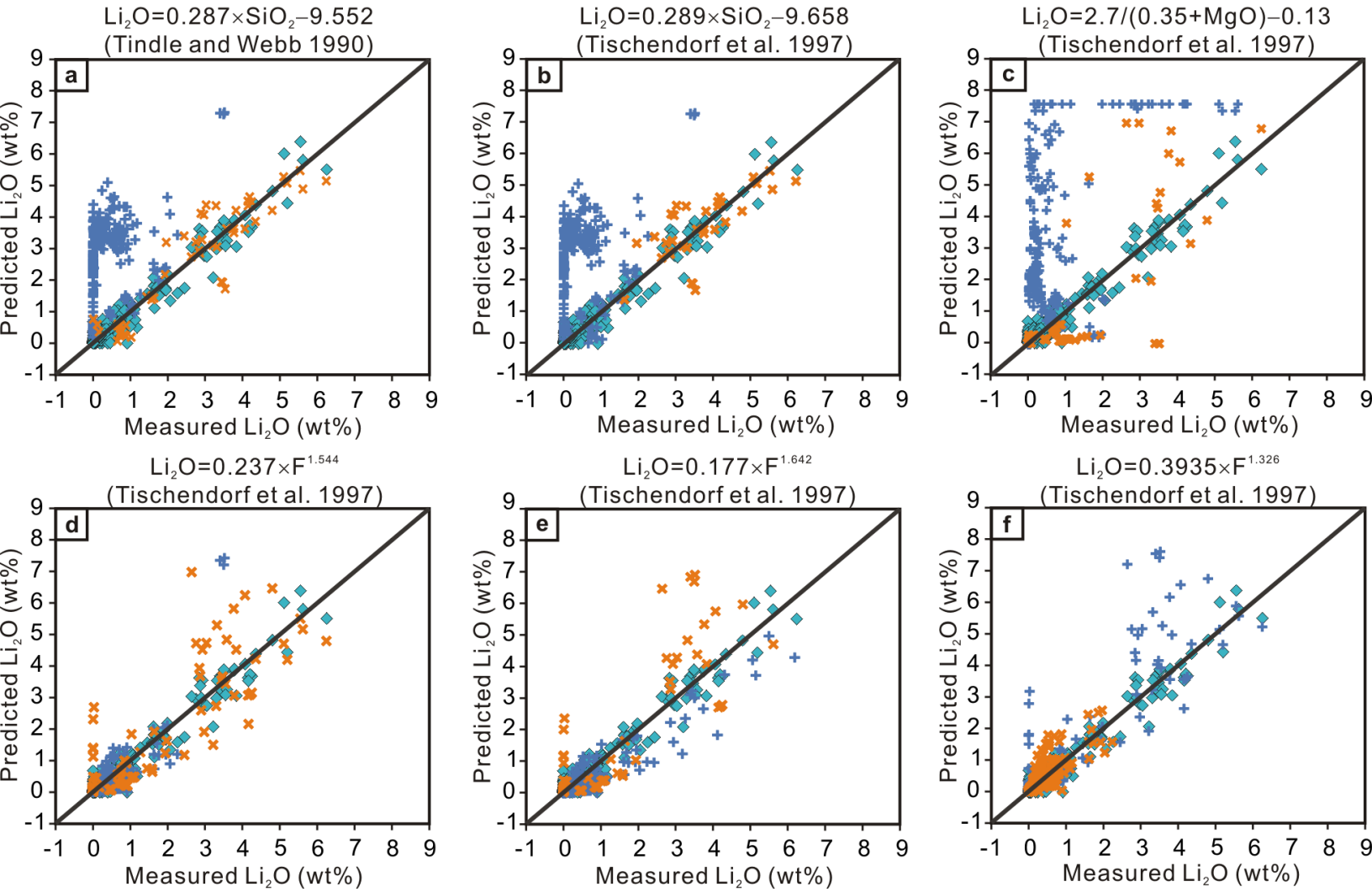

This is the peer-reviewed, final accepted version for American Mineralogist, published by the Mineralogical Society of America.
The published version is subject to change. Cite as Authors (Year) Title. American Mineralogist, in press.
DOI: https://doi.org/10.2138/am-2022-8029. http://www.minsocam.org/

Figure 6

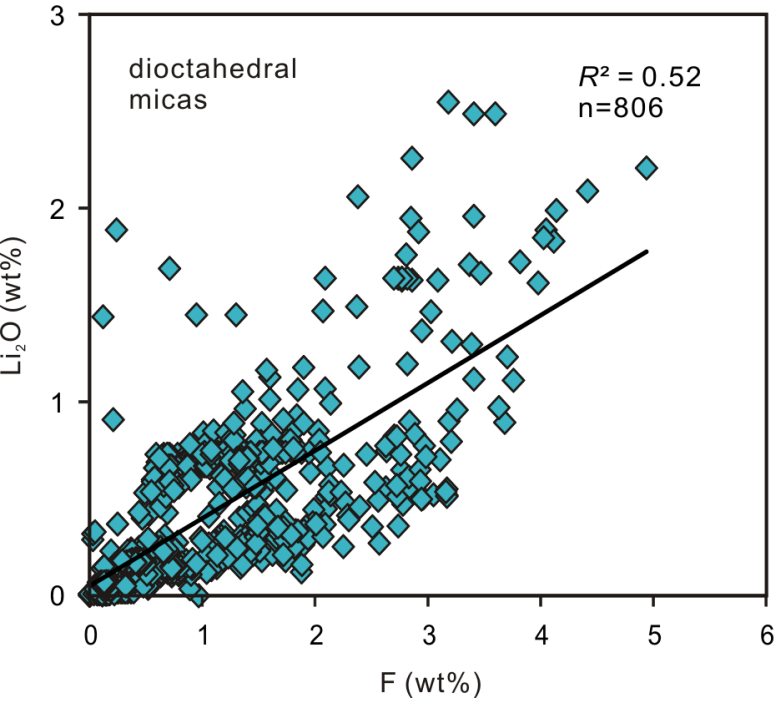

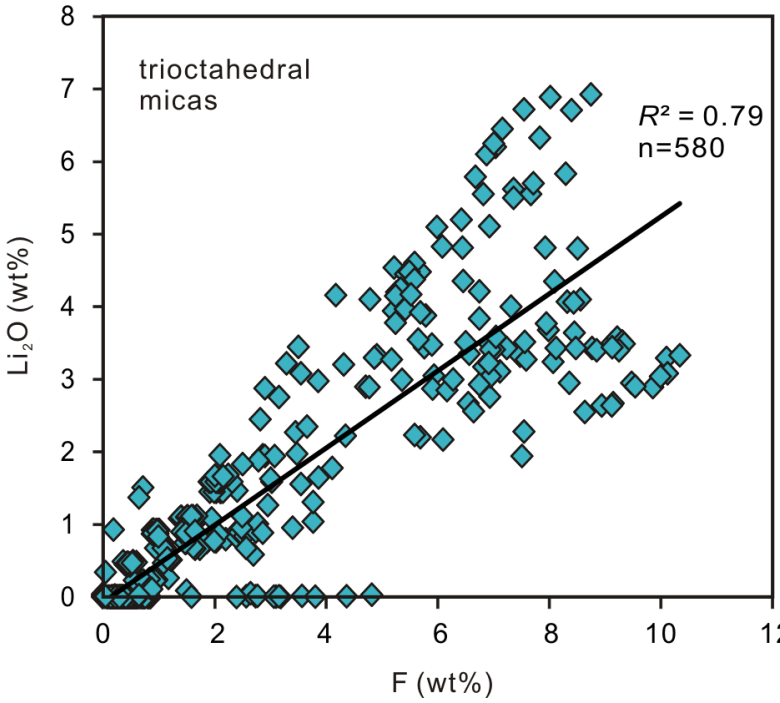

This is the peer-reviewed, final accepted version for American Mineralogist, published by the Mineralogical Society of America.
The published version is subject to change. Cite as Authors (Year) Title. American Mineralogist, in press.
DOI: https://doi.org/10.2138/am-2022-8029. http://www.minsocam.org/

Figure 7

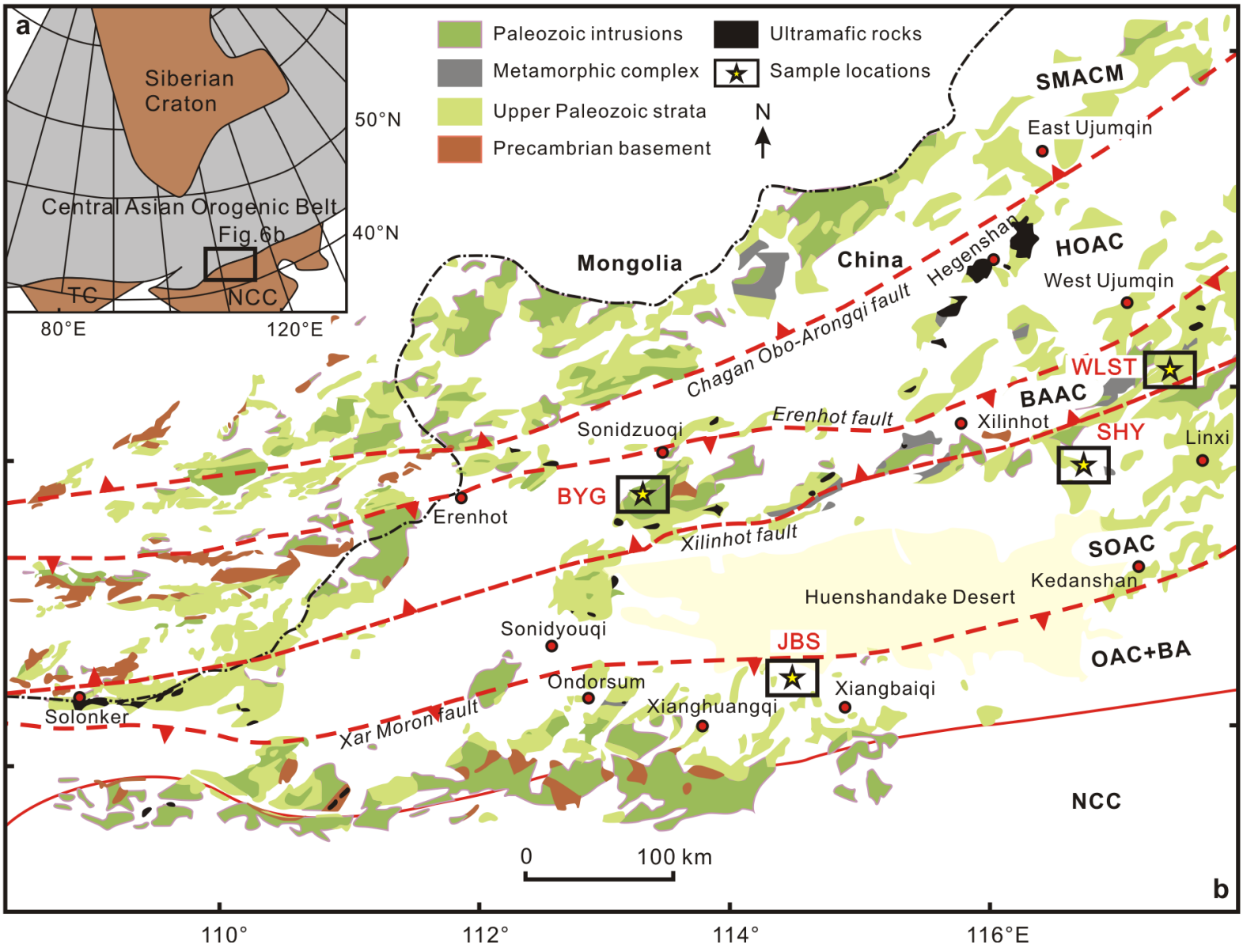

This is the peer-reviewed, final accepted version for American Mineralogist, published by the Mineralogical Society of America.
The published version is subject to change. Cite as Authors (Year) Title. American Mineralogist, in press.
DOI: https://doi.org/10.2138/am-2022-8029. http://www.minsocam.org/

Figure 8

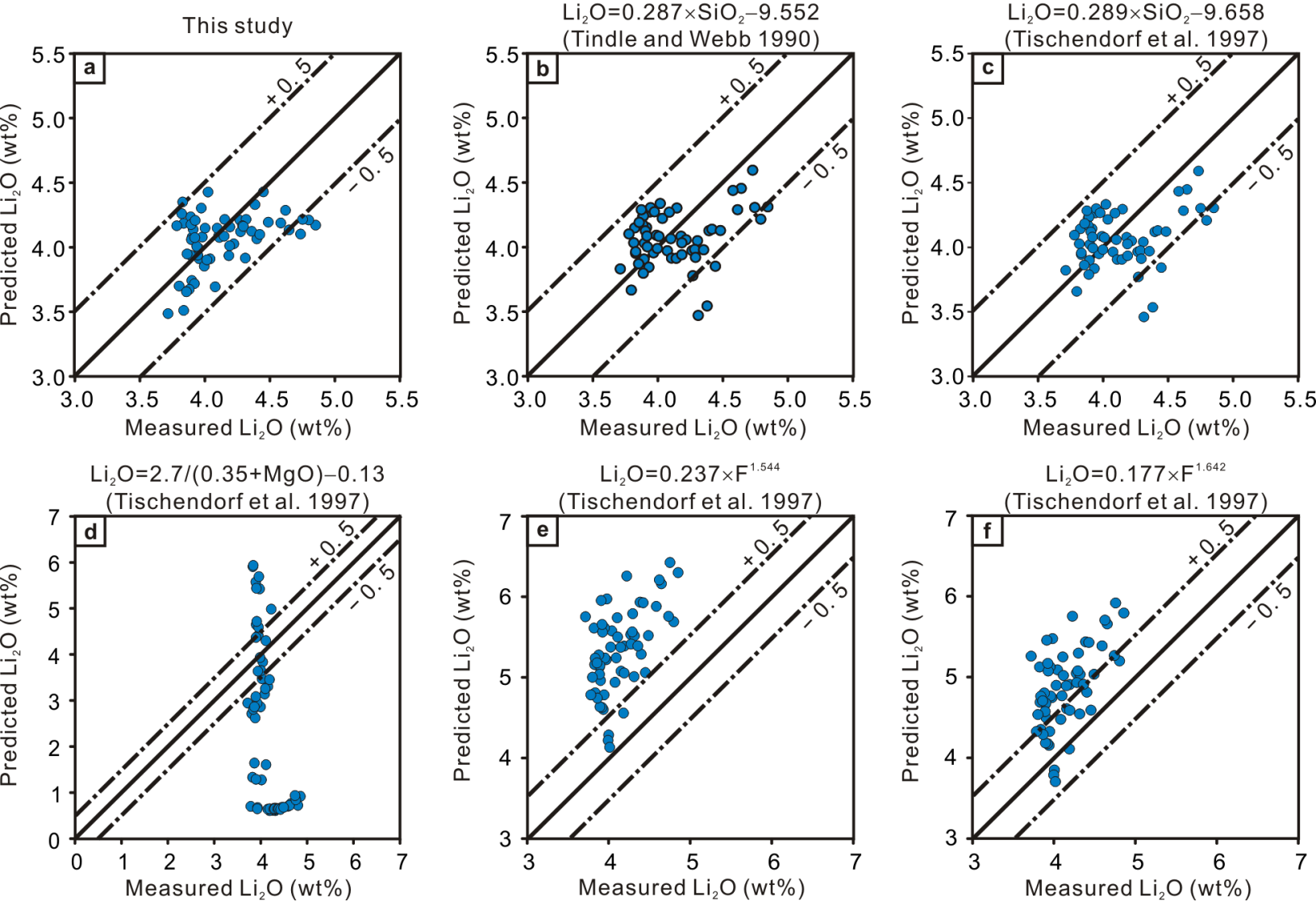

This is the peer-reviewed, final accepted version for American Mineralogist, published by the Mineralogical Society of America.
The published version is subject to change. Cite as Authors (Year) Title. American Mineralogist, in press.
DOI: https://doi.org/10.2138/am-2022-8029. http://www.minsocam.org/

Figure 9

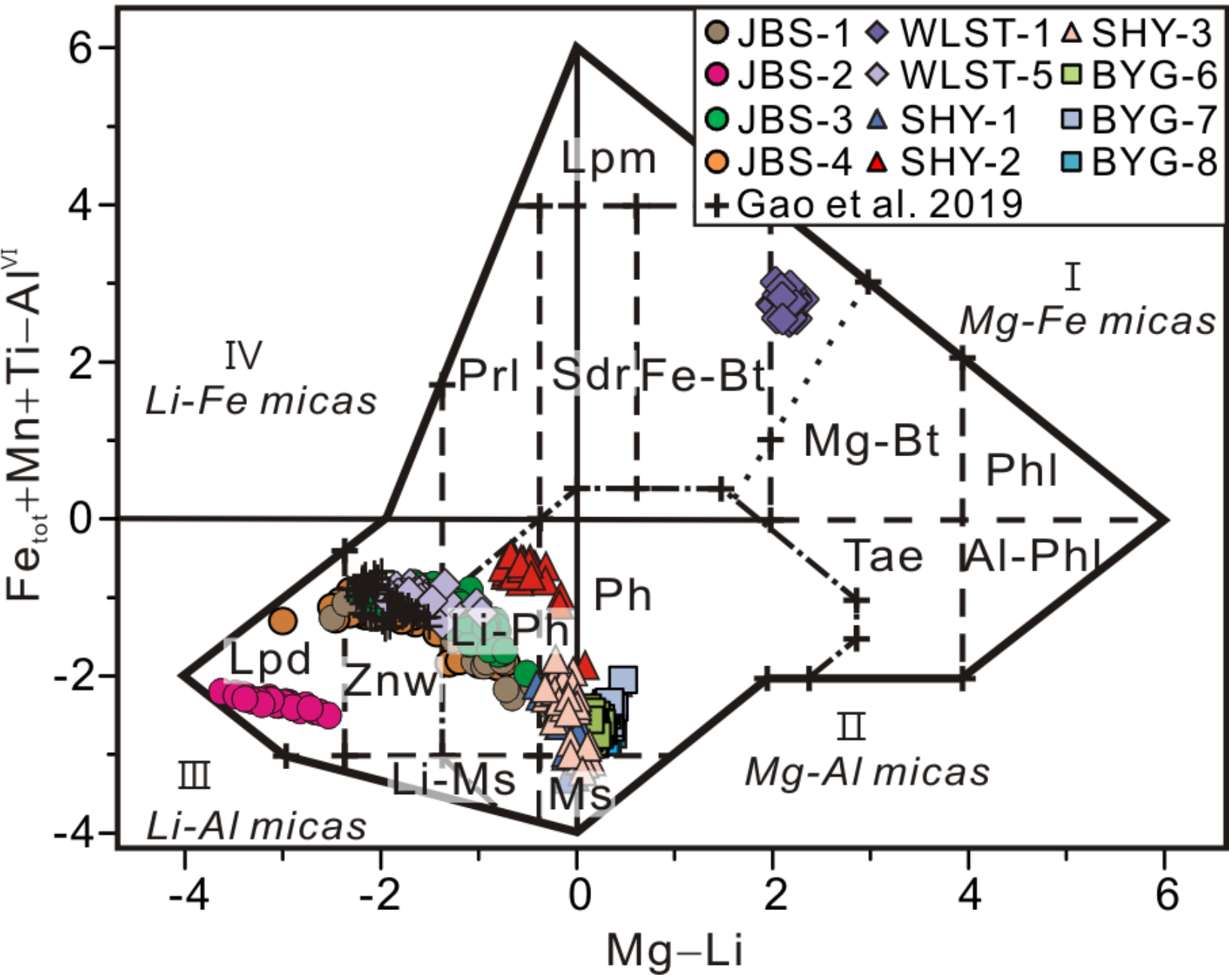

This is the peer-reviewed, final accepted version for American Mineralogist, published by the Mineralogical Society of America.
The published version is subject to change. Cite as Authors (Year) Title. American Mineralogist, in press.
DOI: https://doi.org/10.2138/am-2022-8029. http://www.minsocam.org/

Figure 10